

Review

# Hydrothermal Synthesis of Vanadium Oxide Microstructures with Mixed Oxidation States

Daniel Navas <sup>1,2</sup>

<sup>1</sup> Departamento de Química, Facultad de Ciencias Naturales, Matemática y del Medio Ambiente, Universidad Tecnológica Metropolitana, Las Palmeras 3360, Ñuñoa, Santiago 7800003, Chile; daniel.navas@utem.cl

<sup>2</sup> Instituto de Ciencias Naturales, Facultad de Medicina Veterinaria y Agronomía, Universidad de Las Américas, Sede Providencia, Avenida Manuel Montt 948, Santiago 7500975, Chile

**Abstract:** This review is based on hydrothermal synthetic procedures that generate different vanadium oxide microstructures with mixed oxidation states, where different vanadium ( $V^{5+}$ ) precursors (vanadate, vanadium oxide, vanadium alkoxide, etc.) are used to obtain various types of morphologies and shapes, such as sea urchins, cogs, stars, squares, etc., depending on the amphiphilic molecules (usually surfactants) exhibiting a structural director role containing an organic functional group such as primary amines and thiols, respectively. The performance of sol-gel methodology, where intercalation processes sometimes take place, is crucial prior to the hydrothermal treatment stage to control the  $V^{4+}/V^{5+}$ . In every synthesis, many physical and chemical parameters, such as temperature, pH, reaction time, etc., are responsible for influencing the reactions in order to obtain different products; the final material usually corresponds to a mixed oxidation state structure with different content rates. This feature has been used in many technological applications, and some researchers have enhanced it by functionalizing the products to enhance their electrochemical and magnetic properties. Although some results have been auspicious, there are a number of projects underway to improve the synthesis in many ways, including yield, secondary products, size distribution, oxidation state ratio, etc., to achieve the best benefits from these microstructures in the large number of technological, catalytic, and magnetic devices, among other applications.

**Keywords:** vanadium oxide; hydrothermal treatment; intercalation compounds; sol-gel synthetic procedures; nanoarchitectures; morphology



**Citation:** Navas, D. Hydrothermal Synthesis of Vanadium Oxide Microstructures with Mixed Oxidation States. *Reactions* **2023**, *4*, 1–25. <https://doi.org/10.3390/reactions4010001>

Academic Editor: Dmitry Yu. Murzin

Received: 6 November 2022

Revised: 20 December 2022

Accepted: 22 December 2022

Published: 28 December 2022



**Copyright:** © 2022 by the author. Licensee MDPI, Basel, Switzerland. This article is an open access article distributed under the terms and conditions of the Creative Commons Attribution (CC BY) license (<https://creativecommons.org/licenses/by/4.0/>).

## 1. Introduction

Vanadium oxide nanostructures and microstructures have been researched in many technological applications [1–5], exhibiting amazing morphological characteristics [6] with different architecture types [7], from very well-defined geometric forms [8] to novel spherical clusters consisting of high-density radial arrays made from self-assembled nanotubes [9]. There are several synthetic procedures employed, such as sol-gel processes assisted by amphiphilic surfactants enhanced by hydrothermal treatment; the temperature and the reaction time employed in the latter stage ranges from 180–200 °C and lasts from a few hours up to 10 days [10,11]. The most common  $V^{5+}$  precursors used as starting materials are  $V_2O_5$  (vanadium (V) pentoxide) [12], vanadium alkoxides  $VO(OCH(CH_3)_2)_3$  (vanadium (V) oxytriisopropoxide) [13,14],  $VOCl_3$  (vanadium (V) oxytrichloride) [15], and  $NH_4VO_3$  (ammonium metavanadate) [16,17]. The synthesis commonly requires soft chemical conditions (controlled pH, inert atmosphere, room temperature) and produces the vanadium oxide network, described as an intercalation host lattice [18], where guest species are reversibly inserted between the oxide layers [19–21]. Amphiphilic molecules, such as amphiphilic surfactants, comprising organic functional groups, such as  $RNH_2$  and  $H_2NRNH_2$  (long chain alkyl primary monoamines  $C_nH_{(2n+1)}NH_2$ , diamines  $H_2NC_nH_{(2n)}NH_2$ ), and dipeptides, are commonly intercalated [22–25]. Other surfactants with secondary and tertiary

amines have also been employed [26,27], improving the obtention of different vanadium oxide networks, mainly layered hybrid organic–inorganic intercalation compounds, referred to as organic–inorganic layered composites with novel physical chemical properties. These vanadium oxide layers usually interact under cooperative van der Waals forces [28], mainly the vanadyl bond ( $V = O$ ) and the amine functional group [29]; the most frequent interactions are with hydrogen bonds and ion–dipole forces; these interactions generate different degrees of partial reduction, depending on the amphiphilic functional group [30–33]. Vanadium oxide chemistry is based on shifting the vanadium atom's highest oxidation state to lower ones [34]; the partial reduction often yields mixed oxidation states [35]. The redox reactions performed to obtain different nanostructures are applied to various vanadium oxide ( $V^{5+}$ ) precursors; the reduction proceeds to  $V^{4+}$  and  $V^{3+}$ , and, frequently,  $V^{4+}/V^{5+}$  and  $V^{4+}/V^{3+}$  mixed oxidation states are obtained in the final product [36–38]. These reactions are also associated with the valence, which usually coincides with the oxidation states in the structural lattice. Zabalij et al. [39] conducted a comprehensive study in vanadium oxides focusing on the V ion polyhedral coordination in open extended networks, where the vanadium oxidation state can adopt many coordination polyhedrons with the oxygen atoms, ranging from octahedrons (O), tetrahedrons (T), and trigonal bipyramids (TB), which also exhibit two variants: TB type I and TB type II square pyramids (SP), distorted octahedrons (O), and rectilinear octahedrons (RO) (tetra-, penta- and hexa-coordination), respectively. This wide polyhedron coordination spectrum originates from its unique and bountiful structural chemistry; Figure 1 shows the V ion oscillation from tetrahedron to other polyhedrons with penta- and hexa-coordination.

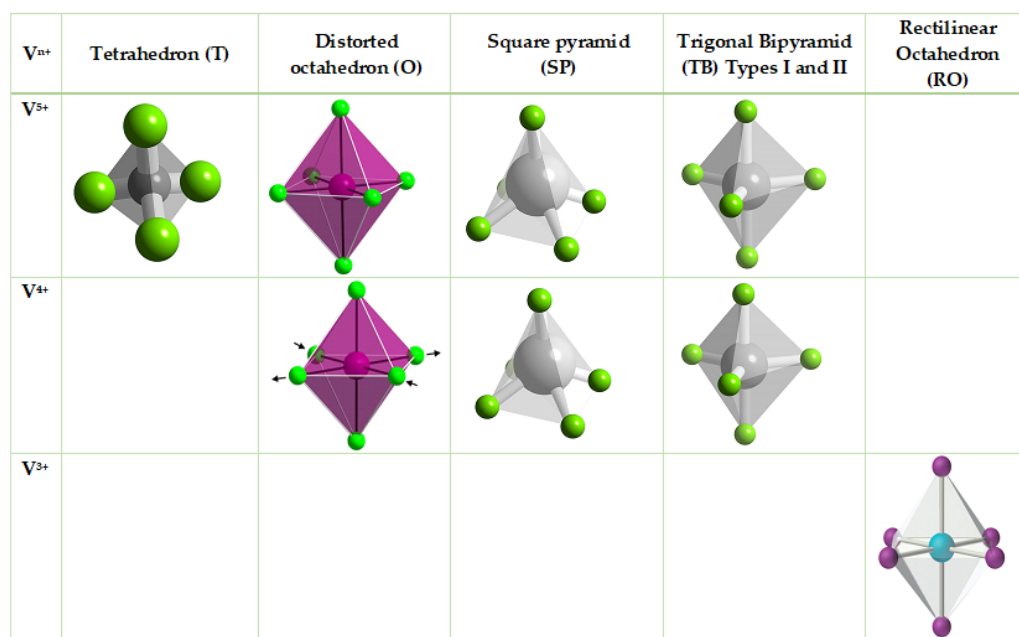
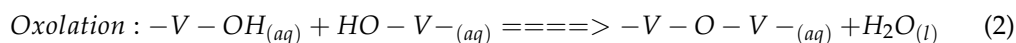
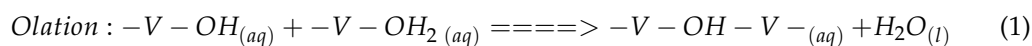


**Figure 1.** Different coordination in vanadium oxide open frameworks, where the  $V^{n+}$  ion may adopt different types of polyhedrons in different structural lattices.

The scheme exhibits a graphical correlation between the vanadium ion oxidation state adopting a preferential coordination polyhedron. For example, the  $V^{5+}$  cation is only located in the tetrahedron polyhedron but also can incorporate the trigonal bipyramid, square pyramid, and distorted octahedra; on the other hand, the  $V^{4+}$  cation appears in the trigonal bipyramid, square pyramid, and distorted octahedra, while the  $V^{3+}$  cation is found solely in the rectilinear octahedra polyhedron. The vanadyl bond ( $V = O$ ) [40] appears in most of the polyhedrons; the only exception is the rectilinear octahedra. Vanadium oxide structural networks are considered to be composed of bonded polyhedrons [41], where chains are created and connected with each other forming 2D (bidimensional) layers

(habitually named sheets) to originate different 3D (tridimensional) networks following the path: polyhedron → chain → layer → tridimensional red; the middle links in the sequence are established as building blocks [42]; therefore, any vanadium oxide network can be defined and classified by the polyhedrons that it is made from. This is the reason that  $V_2O_5$  is described as a shape-shifter, because, once it faces reduction, the  $V^{5+}$  ion coordination changes and a new structural red is obtained. As a result, this modular system material can be used to synthesize, characterize, and tailor-make numerous nano- and microstructures with novel morphologies [43–46]. The aqueous chemistry the  $V^{5+}$  precursors confront under chemical parameters, such as pH, organic polar solvents, concentration, and other species (anions from the  $V^{5+}$  precursor), affect the fashion mode in which the polyhedrons are bonded, influencing the building blocks to create different vanadium oxide networks [47].

Livage., [48] reviewed the condensation reactions that arise at higher concentrations from the aqueous  $V^{5+}$  octahedra precursor, two types of reactions co-exist ololation and oxolation, both reactions are pH reliant and involve hydroxyl and water molecules under nucleophilic addition processes and only take place along the xy planes, both reactions are listed below:



Unfortunately, these reactions do not consider physical parameters, such as temperature and pressure, and chemical parameters such as intercalated guest species, including long alkyl chain surfactants displaying primary monoamines, thiols, and carboxylic acids ( $C_nH_{(2n+1)}NH_2$ ,  $C_nH_{(2n+1)}SH$ , and  $C_{(n-1)}H_{(2n+1)}COOH$ ) organic functional groups [49,50], solvent mixtures with different polarity degrees, and host-guest stoichiometry [51]. The redox reactions will therefore play a major role under hydrothermal treatment [52], where new structural lattices will be formed, depending on the reduction ratio obtained, which will vary in every synthesis [53].

There is a flexible, layered structural host lattice obtained under hydrothermal treatment from different  $V^{5+}$  precursors, which displays a  $V^{4+}/V^{5+}$  mixed oxidation state with different ratios, made of tetrahedral and distorted octahedral/square pyramid mixed valence. This is the main framework of many nano- and microstructures (for example, vanadium oxide nanotubes (VOx-NTs), urchins (VOx-NU), bricks and squares (VOx-MSQ), etc.). This lattice is known as vanadium bronze— $V_7O_{16}^{2-}$ ; it was reported by Wang et al. [54] as  $BaV_7O_{16} \cdot nH_2O$  and consists of  $[V_7O_{16}]$  (six  $VO_6$  distorted octahedral and one  $VO_4$  tetrahedral sites) double layers stacked along the  $[001]$  plane; in-between the layers, the  $Ba^{2+}$  cations and water molecules are intercalated; the structure is made of zig-zag chain trimers consisting of distorted octahedral-coordinated  $V(1)O_6$ - $V(2)O_6$ - $V(1)O_6$  shared-edge atoms; the layer is created when the chain links with other neighboring zig-zag chains by sharing one oxygen atom between the  $V(1)O_6$  —  $V(1)O_6$  octahedral sites. These layers link by sharing common edges, where the octahedral coordination is achieved between the  $V(1)$  site from the upper layer bonding with one oxygen from the  $V(2)$  site from the lower layer, where all the vanadyl bonds are pointing up in the top layer and down in the lower one. Both the distorted octahedral layers are connected with a  $V(3)O_4$  site exhibiting tetrahedral coordination between the  $V(1)O_6$ - $V(2)O_6$  sites in each layer. While the  $V^{4+}$  and  $V^{5+}$  cations occupy the  $V(1)O_6$  and  $V(2)O_6$  sites, the  $V^{5+}$  has a  $V(1)O_6$  site preference, due to a lower symmetry; the lattice has a tetragonal unit cell with red parameters:  $a = 6.1598 \text{ \AA}$ ,  $c = 21.522 \text{ \AA}$ . The structure has been used to simulate the VOx-NTs framework in tetragonal and triclinic modifications [55].

Hellmann et al. [56] proposed another  $[V_7O_{16}]$  structural lattice for tubular morphologies, where the octahedral coordination trimers made of  $V(1)O_5$ - $V(2)O_5$ - $V(1)O_5$  atoms from the zig-zag chains in the double layers are heavily elongated, adopting predominantly a square pyramidal  $VO_5$  coordination. The lattice has a quasi-tetragonal unit cell with red parameters  $a \approx 6.0 \text{ \AA}$ , and the length of the c axis is determined by the self-assembled,

intercalated, long alkyl chain, primary or diamine, between the layers of the stacked  $V_7O_{16}$  framework. There are many structural models based on this structural lattice related to  $VO_x$ -NTs walls [57].

This review focuses on analyzing qualitatively the possible redox reactions at the early stage intercalation sol-gel processes, throughout the hydrothermal treatment that could take place in the different vanadium oxide nano- and microstructures, such as vanadium oxide nanotubes ( $VO_x$ -NTs), nanourchins ( $VO_x$ -NU), micro-squares and crosses ( $VO_x$ -MSQ and  $VO_2$ -MC), nano six-folds (cogs) and nano star-fruits ( $VO_x$ -NC and  $VO_2$ -NSF), exhibiting different degrees of reduction, ranging from mixed oxidation state  $V^{4+}/V^{5+}$  ratios,  $V^{5+}$  complete reduction to  $V^{4+}$ , and mixed oxidation  $V^{3+}/V^{4+}$  ratios, which are associated with different mixed-valence structural lattices, in which  $V_7O_{16}^{2-}$ ,  $VO_2$ , and  $V_6O_{11}$  are obtained, as well as the specific morphology, shape, size distribution, and surface defects, etc., in addition to some approaches to regulate the mixed oxidation  $V^{4+}/V^{5+}$  ratio under soft chemical processes.

## 2. Materials and Methods

The  $V^{5+}$  precursors used are  $V_2O_5$ ,  $VOCl_3$ ,  $VO(OCH(CH_3)_2)_3$ ,  $NH_4VO_3$ , and Xerogel  $V_2O_5 \cdot 1.5 H_2O$ . The most common surfactants employed are mainly long alkyl chain primary mono amines, long alkyl chain thiols, and Pluronic copolymer. The following (Table 1) exhibits some of the synthetic procedures, including some  $V^{5+}$  precursors, the surfactants, and the corresponding structural lattice obtained after hydrothermal treatment.

**Table 1.** Synthetic procedures to obtain different vanadium oxide nano and microstructures under hydrothermal treatment.

| Vanadium Oxide Morphology    | $V^{5+}$ Precursor                           | Surfactant            | Lattice          |
|------------------------------|--|-----------------------|------------------|
| Nanotubes                    | $VO(OCH(CH_3)_2)_3$ [58,59]                  | $C_nH_{(2n+1)}NH_2$   | $V_7O_{16}^{2-}$ |
|                              | $V_2O_5$ and $V_2O_5 \cdot 1.5 H_2O$ [60,61] | $C_nH_{(2n)}(NH_2)_2$ | $V_7O_{16}^{2-}$ |
|                              | $VOCl_3$ [15]                                | $3 < n < 20$          | $V_7O_{16}^{2-}$ |
|                              | $NH_4VO_3$ [16]                              |                       |                  |
| Urchins                      | $VO(OCH(CH_3)_2)_3$ [62]                     | 1-hexadecylamine      | $V_7O_{16}^{2-}$ |
|                              | $V_2O_5$ [63]                                | 1-dodecylamine        | $V_7O_{16}^{2-}$ |
| Squares<br>Crosses           | $NH_4VO_3$ [64,65]                           | 1-hexadecylamine      | $V_7O_{16}^{2-}$ |
|                              | $NH_4VO_3$ [64]                              | 1-hexadecylamine      | $VO_2$           |
| Six-fold cogs<br>Star fruits | $V_2O_5 \cdot 1.5 H_2O$ [66]                 | 1-dodecanethiol       | $V_6O_{11}$      |
|                              | $NH_4VO_3$ [67]                              | 123 Pluronic          | $V_7O_{16}^{2-}$ |

Figure 2 exhibits a scheme sequencing the steps taken to synthesize vanadium oxide nanourchins, which can be applied to nanotubes, squares, and six-folds cogs.

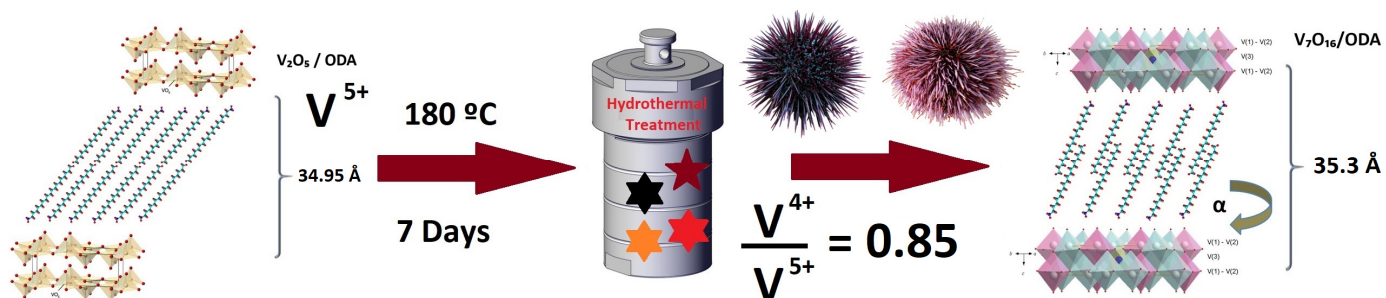


**Figure 2.** Synthetic procedure to obtain vanadium oxide nanourchins, ( $VO_x$ -NU), using  $VO(OCH(CH_3)_2)_3$   $V^{5+}$  precursor and 1-octadecylamine in a sol-gel process enhanced with hydrothermal treatment, where  $V^{5+}$  reduces 46.0% into  $V^{4+}$ , morphing from  $V_2O_5$  to  $V_7O_{16}^{2-}$  structural lattice.

### 3. Results

Table 2 exhibits the V<sup>4+</sup> percentage obtained when the hydrothermal treatment is performed in each synthesis; the reduction is approximately 50.0% in V<sup>4+</sup> VOx-NTs and VOx-NU, 75.0% for squares and bricks (VOx-MSQ), a complete reduction from V<sup>5+</sup> to V<sup>4+</sup> for VOx-MC and VOx-NSF, and sometimes even further to V<sup>3+</sup> in VOx-NC.

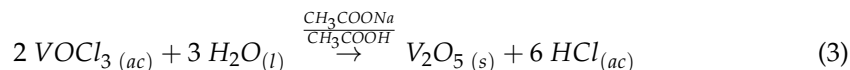
**Table 2.** Reduction percentage of V<sup>4+</sup> from V<sup>5+</sup> associated with each morphology and structural lattice.

| Lattice                                      | V <sup>4+</sup> % | Morphology          |
|--|-------------------|---------------------|
| V <sub>7</sub> O <sub>16</sub> <sup>2-</sup> | 46 to 75%         | VOx-NTs, NU and MSQ |
| VO <sub>2</sub>                              | 100%              | VOx-MC and VOx-NSF  |
| V <sub>6</sub> O <sub>11</sub>               | 66.7%             | VOx-NC              |

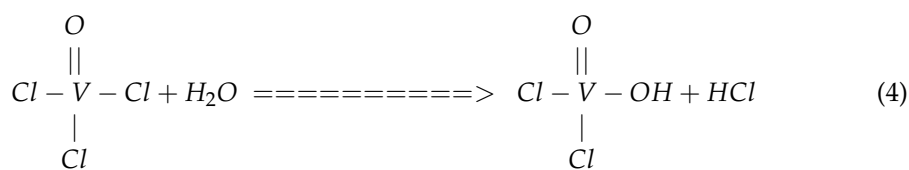
### 4. Discussion

#### 4.1. Vanadium Oxide ((C<sub>n</sub>H<sub>(2n+1)</sub>NH<sub>3</sub>)<sub>2</sub>V<sub>7</sub>O<sub>16</sub> Nanotubes (VOx-NTs)

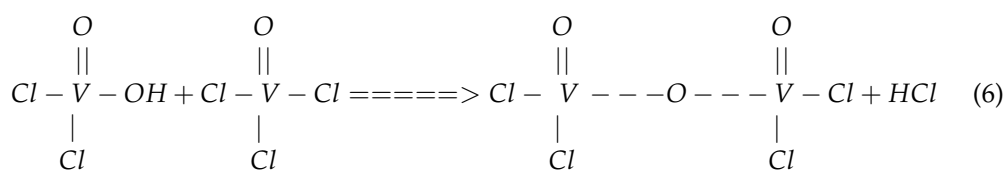
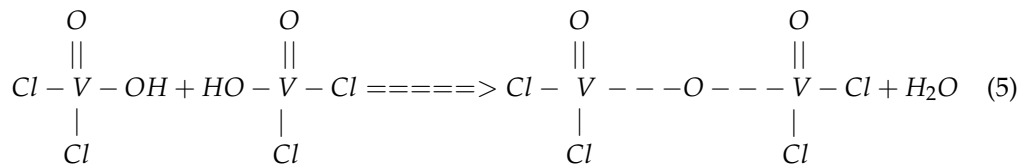
Vanadium oxide nanotubes (often exhibiting micrometric lengths, containing nanometric inner and outer diameters) are synthesized using different vanadium (V) precursors and techniques. For example, V<sub>2</sub>O<sub>5</sub>, NH<sub>4</sub>VO<sub>3</sub>, VOCl<sub>3</sub>, vanadium (V) oxytriisopropoxide, and V<sub>2</sub>O<sub>5</sub>•H<sub>2</sub>O xerogel are directed, with long chain alkyl amines as surfactants, under a sol-gel technique. The first one works straightforwardly as a host lattice to allow guest species to be intercalated, and the others are treated under acid hydrolysis and condensation reactions in order to form the V<sub>2</sub>O<sub>5</sub> host lattice in the presence of long-chain alkyl amines. Some of these precursors will be analyzed below in other microstructures; for example, the VOCl<sub>3</sub> precursor reacts with water and is directed with long alkyl chain amines; the mixture is buffered with CH<sub>3</sub>COONa/CH<sub>3</sub>COOH solution to maintain the pH below 7.0 to produce the layered organic-inorganic nanocomposite; the reduction process is insignificant; and the protonated RNH<sub>3</sub><sup>+</sup> monoamines are intercalated in-between the vanadium oxide layers. The hydrolysis and condensation sol-gel reactions are listed below:



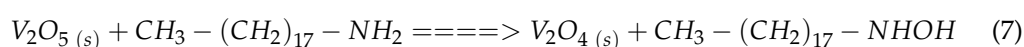
Hydrolysis



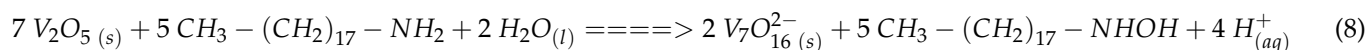
Condensation



The intermolecular forces display a major role in the intercalation processes; the amines are protonated if the pH medium is lower than 7.0 at room temperature. The ion–dipole and dipole–dipole interactions with the vanadyl bond from the host lattice, and the cooperative hydrogen bond interactions between RN-H-O = V, are crucial; on the other hand, the London forces between the hydrophobic hydrocarbon chains allow the establishment of a self-assembled layered RNH<sub>3</sub><sup>+</sup>-V<sub>2</sub>O<sub>5</sub> composite, preventing the reduction process from progressing significantly, even though some undersized V<sup>5+</sup> reduction to V<sup>4+</sup> proceed. The inorganic V<sub>2</sub>O<sub>5</sub> lattice acts like an oxidant agent, accepting electrons and decreasing the vanadium atom oxidation state, while the long alkyl chain primary amine responds as the reducing agent, losing electrons and increasing the number of oxygen atoms in the functional primary amine by replacing a hydrogen atom for a hydroxyl. This can be summarized in the next redox reaction, assuming the structural lattice is V<sub>2</sub>O<sub>5</sub> and 1-octadecylamine is the surfactant.



Hydrothermal treatment at 180 °C for seven days yields VOx-NTs; the reduction process exhibits the V<sup>4+</sup>/V<sup>5+</sup> rate content of 0.85, approximately (46.0% V<sup>4+</sup> and 54.0% V<sup>5+</sup>), the weighted oxidation state responds to 4.54+ (V<sup>4.54+</sup>). Therefore, a mixed oxidation-state vanadium oxide lattice is formed; in these nanotubes, the self-assembled long alkyl chain primary amines are still embedded (intercalated) inside the vanadium oxide layers; therefore, the intermolecular forces previously mentioned are once again responsible for preventing a complete reduction from V<sup>5+</sup> to V<sup>4+</sup>. The flexible host lattice rolls up, acquiring the nanotube morphology ((C<sub>n</sub>H<sub>(2n+1)</sub>NH<sub>3</sub>)<sub>2</sub>V<sub>7</sub>O<sub>16</sub> with 3 < n < 21). The transmission electron micrographs in Figure 3 illustrate the morphology; the tubular walls of the VOx-NTs are composed of a (C<sub>n</sub>H<sub>(2n+1)</sub>NH<sub>3</sub>)<sub>2</sub>V<sub>7</sub>O<sub>16</sub> layered framework made of zig-zag chains, consisting of square pyramids that shares their edges, whereas the V(2)O<sub>5</sub> site is surrounded by two V(1)O<sub>5</sub> sites, generating a trimer which is connected with another chain by sharing an oxygen atom creating a layer where all the vanadyl bonds are pointing up in the pyramid apex direction. This layer is connected with another one featuring the same structure, pointing in the opposite direction, by sharing a tetrahedral V(3)O<sub>4</sub> site in-between them, conferring on the framework some robustness and flexibility; the red triclinic unit cell parameters are a = 6.16 Å, b = 6.17 Å, and c = 19.1 Å, with α = 96.14°, β = 92.82°, and γ = 90.07° [68]. The V<sup>4+</sup> = O vanadyl bond has been reported as being localized in the tetrahedral V(3)O<sub>4</sub> sites [69]. The buffer CH<sub>3</sub>COONa/CH<sub>3</sub>COOH and chloride anions must be removed before the hydrothermal treatment; otherwise, it will interact with the embedded amines during the reaction at 180 °C, causing the self-assembled amines to displace from the host lattice, which facilitates a further reduction that could result in V<sup>4+</sup>. A simple reaction is listed below (using 1-octadecylamine (ODA)):



#### 4.2. Vanadium Oxide ((C<sub>n</sub>H<sub>(2n+1)</sub>NH<sub>3</sub>)<sub>2</sub>V<sub>7</sub>O<sub>16</sub> Nanourchins (VOx-NU)

Vanadium oxide nanourchins (VOx-NTs) are synthesized using the same alkoxide synthetic route as VOx-NTs. O'Dwyer and Roppolo et al. used the V<sup>5+</sup> precursor VO(CH(CH<sub>3</sub>)<sub>2</sub>)<sub>3</sub> [70,71]. Even though the same stoichiometry is used 2:1 (alkoxide: long alkyl chain primary monoamine), the quantity and solvent ratios employed in the synthesis are different; therefore, the surfactants' arrangement in this solvent:medium ratio might explain the morphology of the high-density, nanotubes radial array spherical clusters; the sol–gel process is directed by long alkyl chain primary monoamines, for example, 1-hexadecylamine, 1-dodecylamine, and 1-octadecylamine. The synthesis is performed under inert atmospheric conditions (Argon environment) in a solvent ethanol/water mixture medium. In the obtention of a layered intercalation inorganic–organic compound, where the long alkyl chain primary amines are intercalated in a self-assembled configu-

ration in-between the layers of a  $V_2O_5$  host lattice, the process is concealed by the same intermolecular interactions explained previously in  $VO_x$ -NTs, the sol-gel hydrolysis and condensation reactions are listed below.

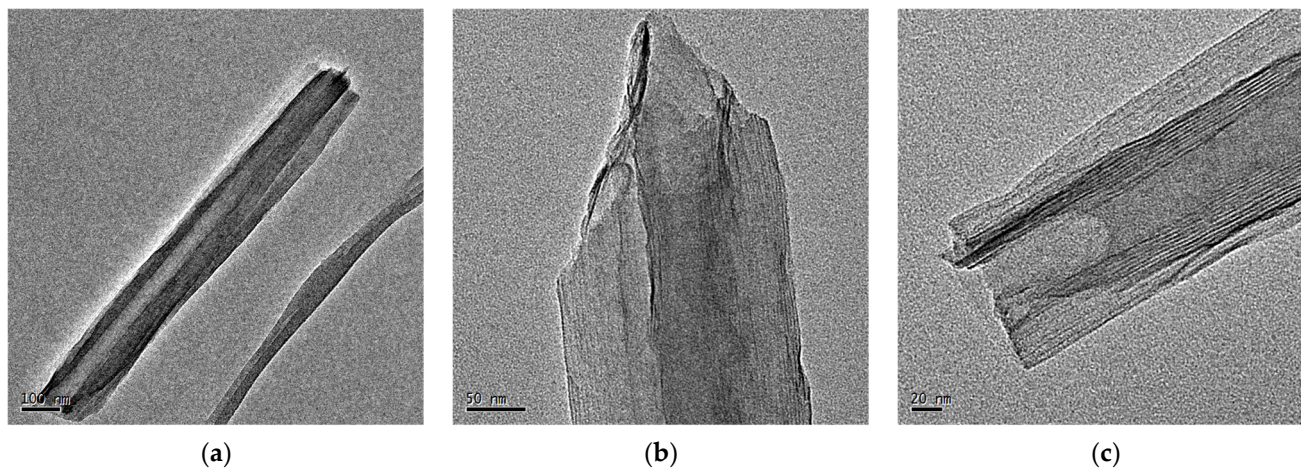
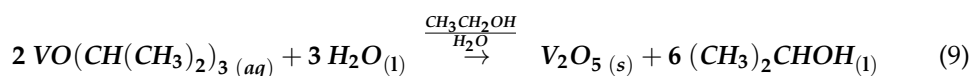
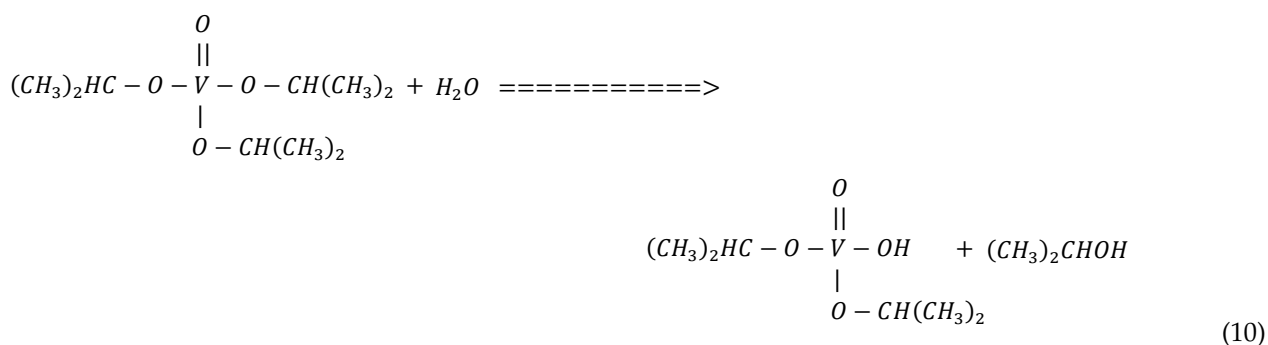


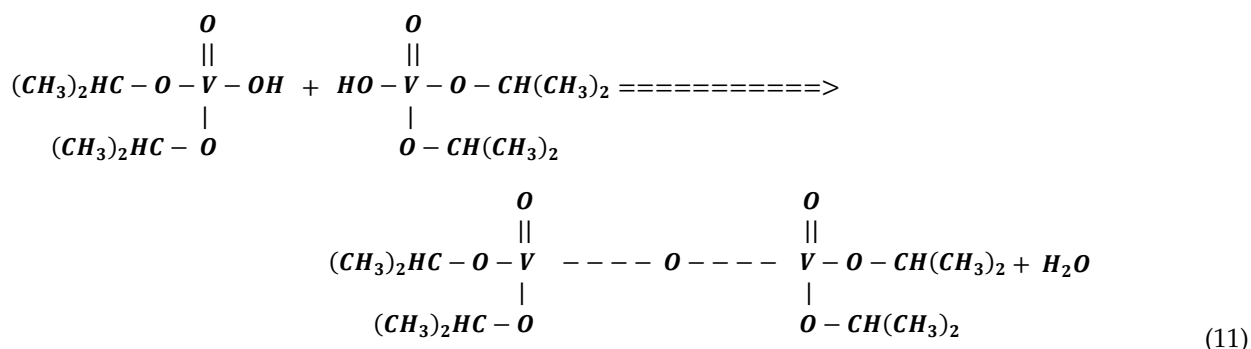
**Figure 3.** TEM micrographs of vanadium oxide nanotubes  $VO_x$ -NTs: (a) single nanotube exhibits the micrometric, hollow center inner and outer diameter; (b) nanotube walls made of  $V_7O_{16}^{2-}$  lattice embedded with self-assembled long alkyl chain amines; the dark fringes correspond to  $V_7O_{16}^{2-}$ ; host lattice colorless fringes in-between are associated with the embedded organic amines; and (c) tubular open-ended package.



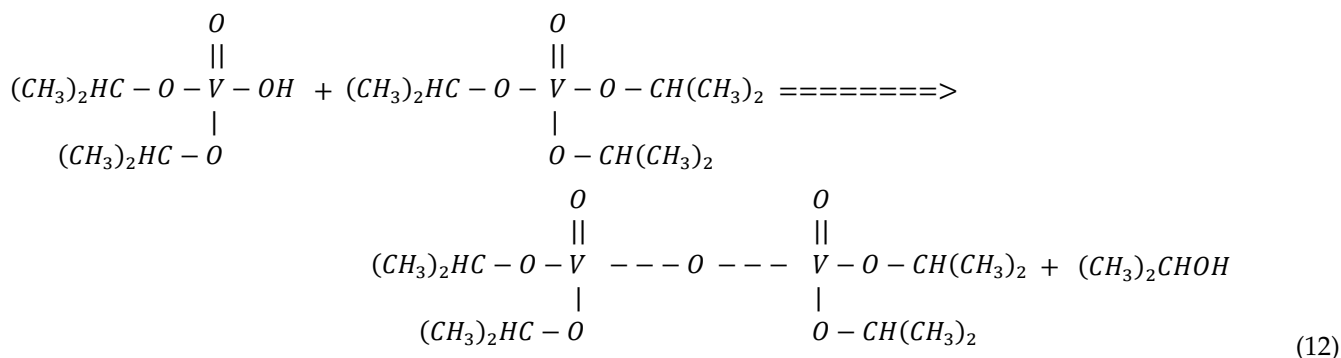
Hydrolysis



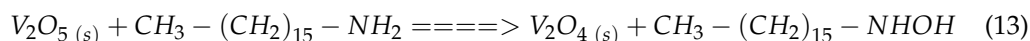
Condensation 1



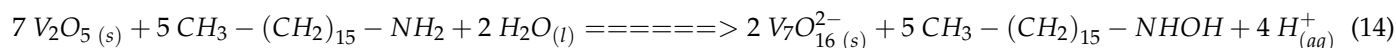
Condensation 2



The inorganic–organic layered intercalation compound features a minor reduction process at room temperature from  $V^{5+}$  to  $V^{4+}$ , where the  $V_2O_5$  host displays an oxidant agent role and the long alkyl chain primary monoamines a reducing agent role; the intermolecular interactions prevent a major reduction degree taking place. The next redox reaction exhibits this process.



The hydrothermal treatment at 180 °C over seven days creates the nanourchin spherical clusters. In this process, many different reactions take place; the  $V^{5+}$  to  $V^{4+}$  reduction is significant and ranges from 46 to 50% (the weighted oxidation state is  $V^{4.54+}$  and  $V^{4.5+}$ ); the temperature and pressure might be key factors transitioning the structural lattice from  $V_2O_5$  to  $V_7O_{16}^{2-}$ ; and the inorganic–organic layered intercalation compound retains the self-assembled long alkyl chain primary amines inside the  $V_7O_{16}^{2-}$  layers ( $(C_nH_{(2n+1)}NH_3)_2V_7O_{16}$  with  $11 < n < 19$ ). Therefore, the intermolecular interactions are controlling the  $V^{4+}/V^{5+}$  ratio from 0.85 to 1.0. The morphology displays a tubular configuration, which is also self-assembled in spherical clusters. The structural lattice is the same framework studied previously on the vanadium oxide nanotubes; the redox reaction below exhibits this process, assuming the long alkyl chain primary monoamines (1-hexadecylamine (HDA)) are acting as reducing agents.

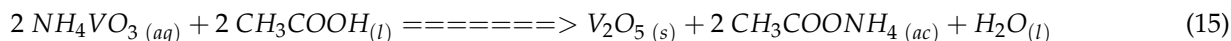


Perera et al. [63] synthesized VOx-NU using 10 mmol  $V_2O_5$  precursor with 10 mmol 1-hexadecylamine under strong agitation in 40 mL of deionized water for 48 h; the yellow suspension was Teflon-aligned under hydrothermal treatment for seven days, and spherical clusters with high-density nanotubes were obtained, in which the amines are intercalated in-between the  $V_7O_{16}^{2-}$  layers interacting under van der Waals forces. The next set of SEM micrographs in Figure 4 exhibits the spherical clusters (nanourchin-obtained) after hydrothermal treatment, which features the high-density nanotube radial arrays, for more detailed scanning electron micrographs see supplementary information Figure S1.

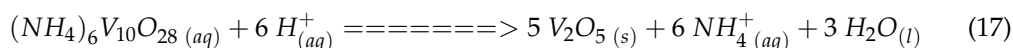
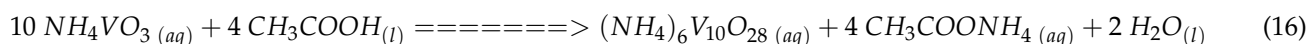
#### 4.3. Vanadium Oxide $(NH_4)_2V_7O_{16}$ Micro-Squares (VOx-MSQ) and $VO_2$ Micro-Crosses (VOx-MC)

Vanadium oxide micro-squares VOx-MSQ ( $(NH_4)_2V_7O_{16}$ ) were obtained by Navas et al. [64], featuring the  $V_7O_{16}^{2-}$  structural lattice of  $BaV_7O_{16} \cdot nH_2O$  (a tetragonal unit cell with red parameters  $a \approx 0.617$  and  $c = 21.522$  Å) made of double, upper and lower layers of zig-zag chains, which are interconnected with other zig-zag chains by sharing one oxygen atom. Each chain consists of distorted octahedral  $VO_6$  trimers (occurring when the V(1) site from the upper layer coordinates with an oxygen atom of the V(2) site from the lower layer, if both layers are close enough). These are linked with a V(3)O<sub>4</sub> site with tetrahedral coordination located in-between the layers, which generates the final stacked layered framework, where the ammonia polycation is intercalated. The rolling process

is suppressed throughout the hydrothermal treatment; therefore, no tubular morphology arises. Nevertheless, a square morphology is obtained; the synthesis employs ammonium metavanadate ( $\text{NH}_4\text{VO}_3$ ) as the  $\text{V}^{5+}$  precursor and 1-hexadecylamine as the amphipathic organic template; the stoichiometry ( $\text{NH}_4\text{VO}_3$ : 1-hexadecylamine) used is 2:1; the pH is adjusted using  $\text{CH}_3\text{COOH}$  (acetic acid) in a  $\text{CH}_3\text{CH}_2\text{OH}/\text{H}_2\text{O}$  solvent mixture to facilitate the sol-gel process, even though the aqueous vanadate reactions are extensive and intricate. An abbreviated reaction is exhibited below:



The  $\text{V}^{5+}$  ( $\text{NH}_4\text{VO}_3$ ) precursor reacts with acetic acid and water; the orange color suspension of the decavanadate polyanion ( $\text{V}_{10}\text{O}_{28}^{6-}$ ) is obtained; it consists of ten edge-sharing  $\text{VO}_6$  octahedra, which act as building-block clusters at  $\text{pH} < 2.0$ , precipitating as a layered organic-inorganic intercalation compound made of  $\text{V}_2\text{O}_5$  host lattice-containing, intercalated, self-assembled long alkyl chain primary monoamines guests; both reactions are listed below.



The formation of the structural lattice could be conducted under two reactions, hydrolysis and condensation, because the pH reduces the coordination increases; therefore, the reaction could be represented below.

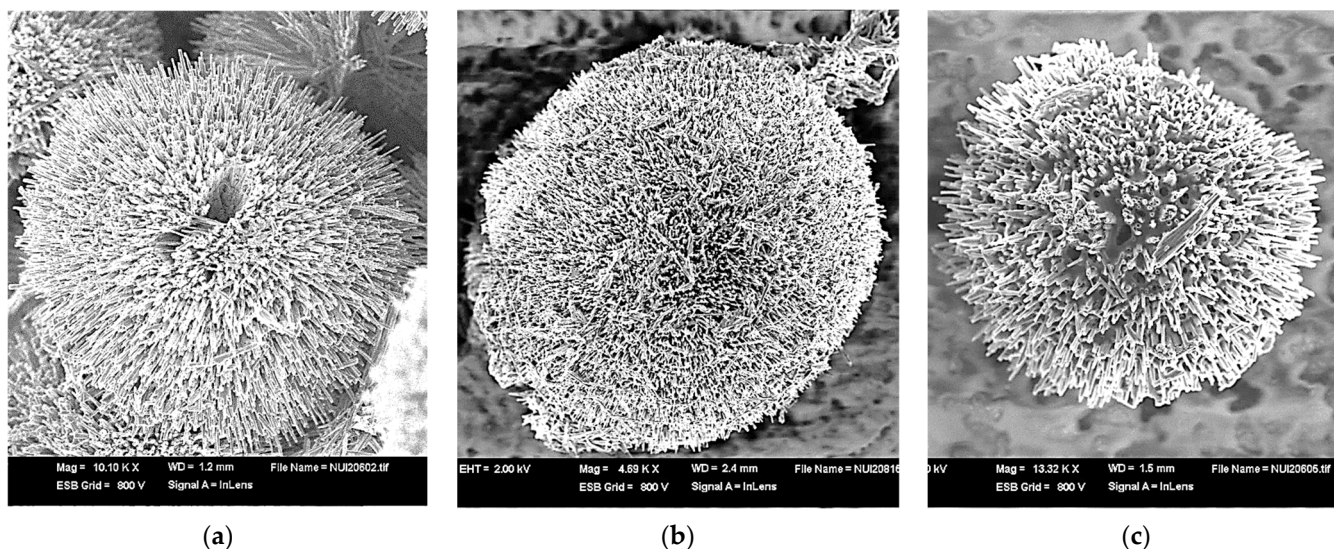
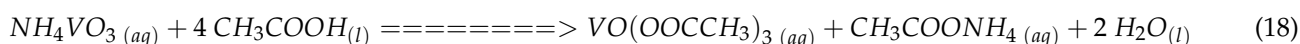
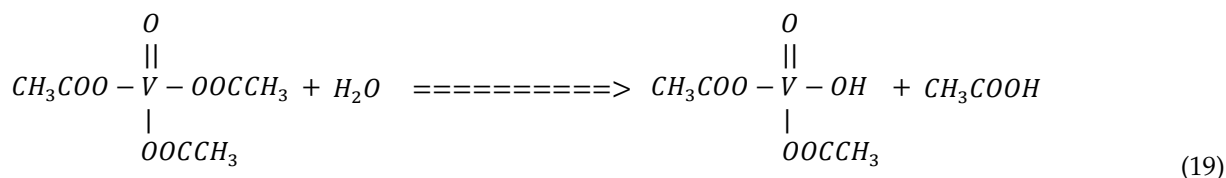


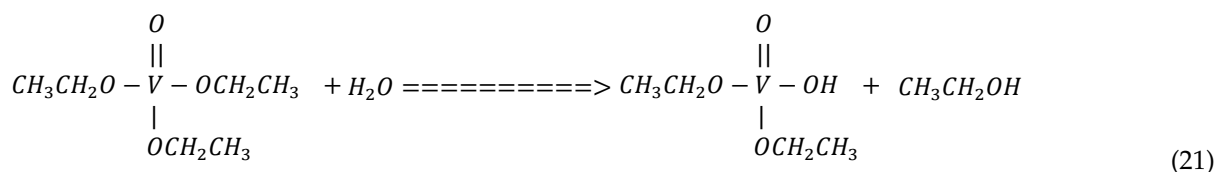
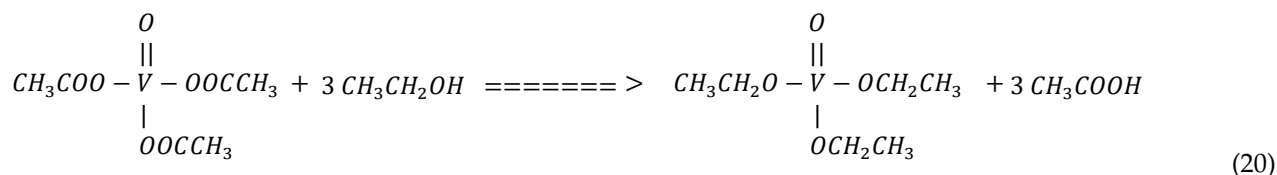
**Figure 4.** SEM micrographs of vanadium oxide ( $\text{C}_{18}\text{H}_{37}\text{NH}_3$ ) $_2\text{V}_7\text{O}_{16}$  high-density  $\text{VO}_x$ -NTs radial array spherical clusters (nanourchins,  $\text{VO}_x$ -NU): (a) hole-centered vanadium oxide nanourchin; (b) heavy-sized vanadium oxide nanourchin; (c) isolated vanadium oxide nanourchin.



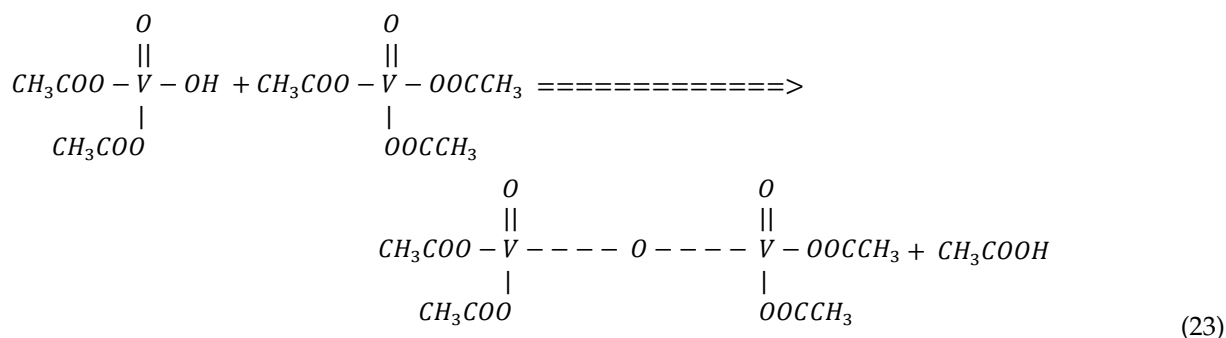
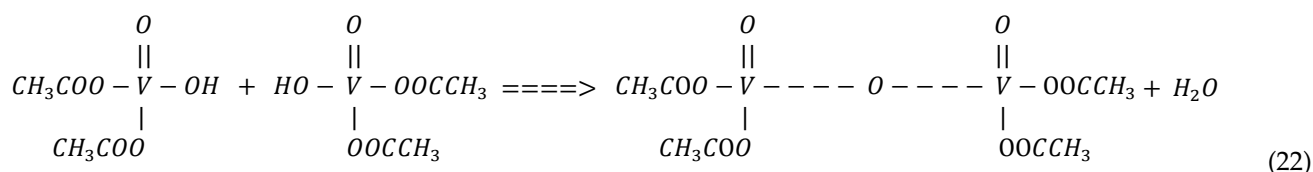
Hydrolysis



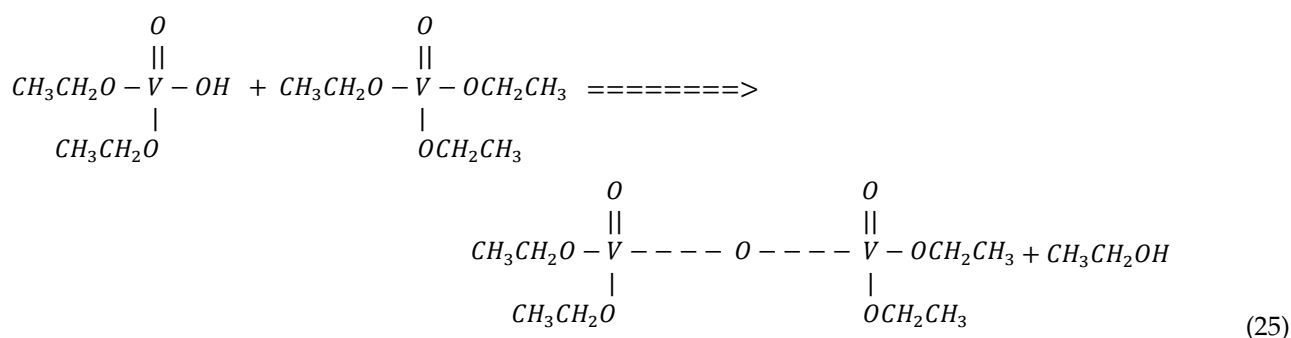
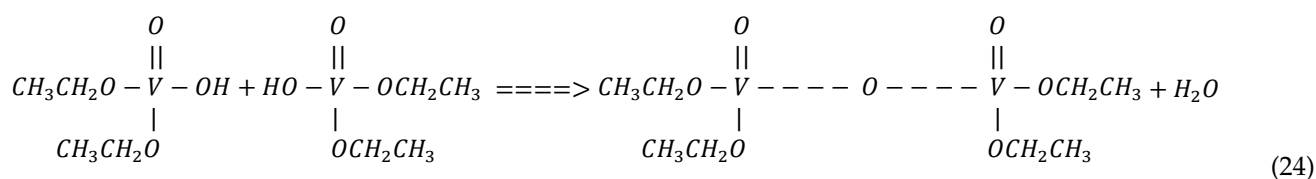
Ethanol might also have taken part in the hydrolysis reactions; for example, if 3 mol of ethanol had interexchanged with 3 mol of acetate polyanion, this might accelerate this process:



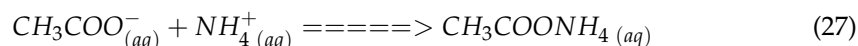
Condensation



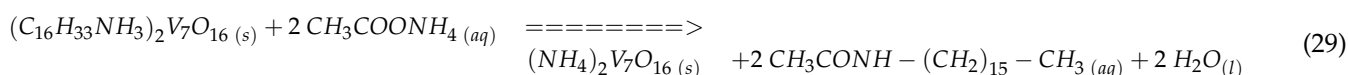
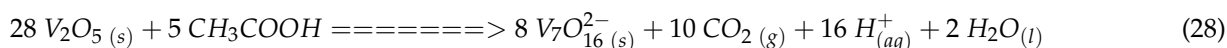
The same process might also take place simultaneously, involving the ethanolic precursors:



At room temperature, the sol–gel process does not generate a major degree of reduction from  $V^{5+}$  to  $V^{4+}$ , and intermolecular forces prevent the reduction taking place as reviewed in the previous  $V_7O_{16}$  structures. The layered inorganic–organic intercalation compound remains stable; the long alkyl chain amine protonation ( $C_{16}H_{33}NH_3^+$  conjugated acid) with acetic acid at a lower pH generates an exchange reaction. The  $NH_4^+$  polycations are replaced with  $C_{16}H_{33}NH_3^+$  inside the host lattice by reacting with acetate ( $CH_3COO^-$  conjugated base), forming the neutral  $CH_3COONH_4$ . The acid–base set of reactions are described below.



The reduction process in the  $V^{4+}$  content is 73.0% in VOx-MSQ after hydrothermal treatment is performed at 180 °C. There are many factors involved: the disintercalation from the self-assembled long alkyl chain primary monoamines; the concentrated acetic acid playing a fundamental role as a reductant agent, and also reacting with the long alkyl chain primary monoamines creating long alkyl chain secondary monoamides; the structural lattice  $V_7O_{16}^{2-}$  hosts the remaining  $NH_4^+$  polycations to neutralize the negative charge under intercalation; therefore, the rolling effect is hindered, and the tubular morphology is missing. Instead, the flat squared morphology made of stacked pillared intercalated  $(NH_4)_2V_7O_{16}$  layered composite is obtained. Even though some intermolecular forces are still present, the London forces between the carbon long alkyl chains from the primary monoamines are absent; the interlayer distance is shortened, blocking the rolling process, and allowing the reduction to increase. The cooperative hydrogen bonds and ion-dipole interactions between the ammonium polycations with the vanadyl bonds from the  $V_7O_{16}^{2-}$  lattice prevent the entire reduction to  $VO_2$ ; the  $V^{4+}/V^{5+}$  ratio is 2.745 (73.3%  $V^{4+}$  and 26.7%  $V^{5+}$ ). The quantification was performed using a calibrated permanganometric titration; the weighted oxidation state was 4.267+ ( $V^{4.267+}$ ), similar to  $BaV_7O_{16} \cdot nH_2O$  structure, which reported a 4.29+ ( $V^{4.29+}$ ) weighted oxidation state (71.0%  $V^{4+}$  and 29.0%  $V^{5+}$ , with a  $V^{4+}/V^{5+}$  ratio of 2.45). The next set of reactions exhibits this redox process and the long alkyl chain primary monoamines disintercalation:



The SEM and TEM micrographs from the  $(NH_4)_2V_7O_{16}$  are exhibited below in Figures 5 and 6, which feature the micrometric square morphology.

Wang et al. [65] reported the same synthesis previously described, modifying the amount of water used, and increased the aging time up to five days. The hydrothermal treatment was performed at 180 °C over five consecutive days; the VOx-MSQ ( $(NH_4)_2V_7O_{16} \cdot 3H_2O$ ) displays the same square morphology; the  $V^{4+}/V^{5+}$  ratio is 2.448, which responds to a weighted oxidation state of 4.29+ ( $V^{4.29+}$ ) distributed between 71.0%  $V^{4+}$  and 29.0%  $V^{5+}$ . The structure differs from its predecessor on the red lattice parameters, where the unit cell is triclinic ( $a = 6.1008 \text{ \AA}$ ,  $b = 12.1826 \text{ \AA}$ , and  $c = 17.8954 \text{ \AA}$ , with  $\alpha = 88.8205^\circ$ ,  $\beta = 84.0988^\circ$ , and  $\gamma = 89.8291^\circ$ ) and is made of double upper and lower layers of zig-zag chains that are interconnected by sharing one oxygen atom with the  $V(1)O_5$  sites. Each chain consists of square pyramid  $VO_5$  trimers displaying  $V(1)O_5$ - $V(2)O_5$ - $V(1)O_5$  edge-sharing modes (the elongated octahedral coordination is excessively far between the sites  $V(1)O_5$  from the upper and  $V(2)O_5$  from the lower layers); the layers are linked via the  $V(3)O_4$  site, with tetrahedral coordination in-between the layers that generates the final, stacked layered framework where the ammonia polycation is intercalated.

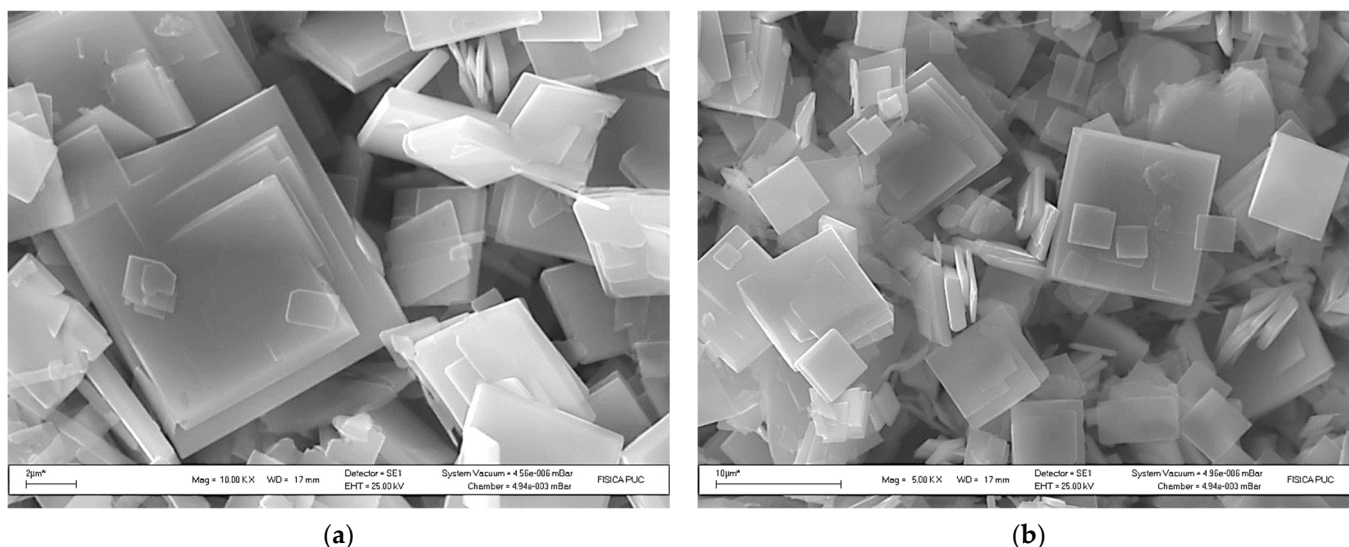


**Figure 5.** SEM micrographs of vanadium oxide  $(\text{NH}_4)_2\text{V}_7\text{O}_{16}$  micro-squares (VOx-MSQ): (a) detailed square morphology; and (b) square morphology with different sizes.

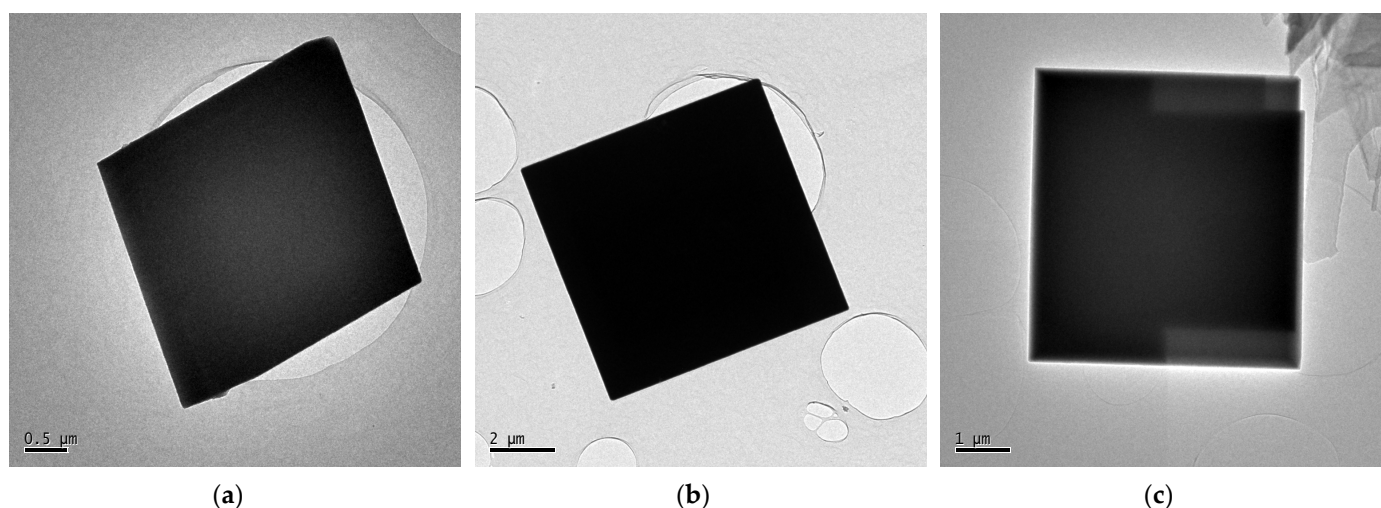
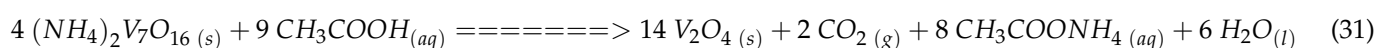
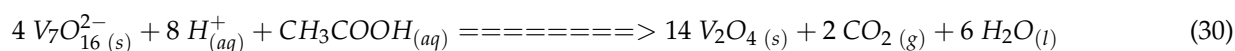


**Figure 6.** TEM micrographs of vanadium oxide  $(\text{NH}_4)_2\text{V}_7\text{O}_{16}$  micro-squares (VOx-MSQ): (a) tilted microstructure square morphology; (b) isolated microstructure square morphology; (c) overlapped VOx-MSQ.

Vanadium oxide micro-crosses (VOx-MC) are obtained when hydrothermal treatment is performed for longer periods of time (over 10 days); the reducing agent, acetic acid, reduces the  $\text{V}_7\text{O}_{16}^{2-}$  oxidant agent entirely into the  $\text{VO}_2$  structural lattice; the vanadium atom oxidation state is 4+ ( $\text{V}^{4+}$ ); the disintercalation of the  $\text{NH}_4^+$  polycations is achieved to create ammonium acetate. Therefore, without any intermolecular forces, a complete reduction from  $\text{V}^{5+}$  to  $\text{V}^{4+}$  is achieved; the square to cross morphology transformation suggests the  $(\text{NH}_4)_2\text{V}_7\text{O}_{16}$  micro-squares have split in four symmetrical  $\text{VO}_2$  folds; a possible redox reaction and the main  $\text{NH}_4^+$  disintercalation reactions are exhibited.



The next set of SEM micrographs in Figure 7 displays the VO<sub>2</sub> micro-cross (VO<sub>x</sub>-MC) morphology once the intercalation compound has been dismantled. The supporting information exhibits more detailed SEM and TEM micrographs of VO<sub>x</sub>-MC in Figures S2 and S3.

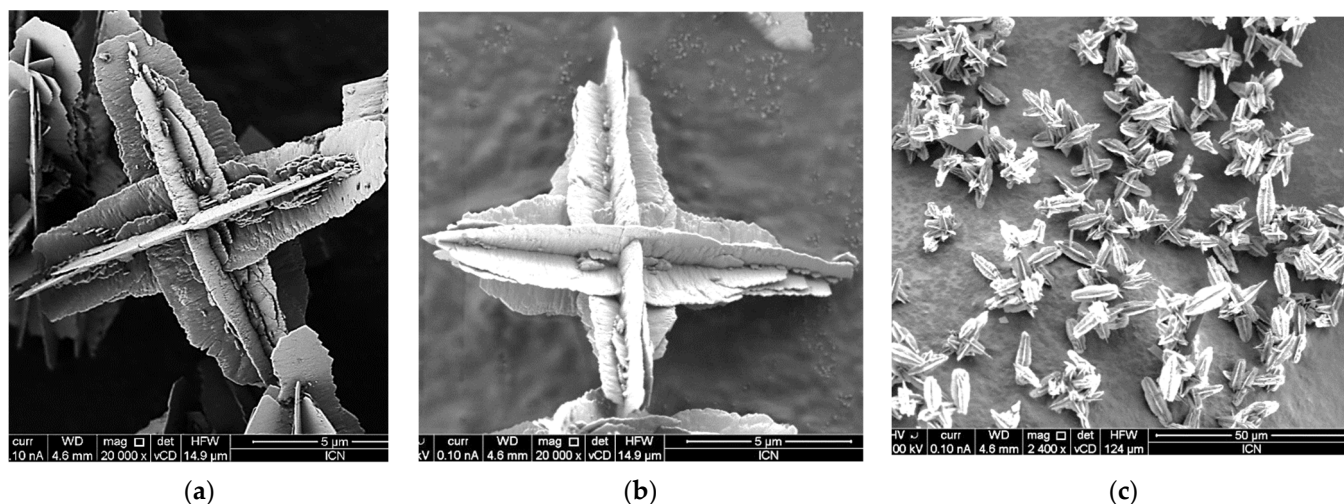
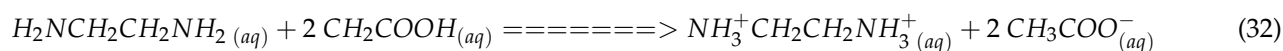
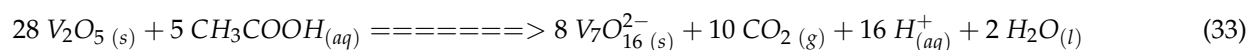


**Figure 7.** SEM micrographs of vanadium oxide VO<sub>2</sub> micro-crosses (VO<sub>x</sub>-MC): (a,b) detailed cross morphology exhibiting four split VO<sub>2</sub> folds; (c) clustered micro-crosses and long scan exhibiting the yield and morphological aspect.

Roppolo et al. [71] synthesized a (EnH<sub>2</sub>)<sub>2</sub>V<sub>7</sub>O<sub>16</sub> (VO<sub>x</sub>-MSQ) structure with a V<sub>2</sub>O<sub>5</sub> (V<sup>5+</sup> precursor) and ethylenediamine (H<sub>2</sub>NCH<sub>2</sub>CH<sub>2</sub>NH<sub>2</sub>), employing a 2:1 molar ratio, using an ethanol/water mixture for 24 h; the pH is controlled during the sol-gel process with acetic acid (CH<sub>3</sub>COOH) at different values from 3, 4, 5, to 7. The (EnH<sub>2</sub>)<sub>2</sub>V<sub>7</sub>O<sub>16</sub> squares are obtained applying hydrothermal treatment for seven days at 180 °C; the structure has a triclinic unit cell with red parameters: a = 6.167 Å, b = 6.170 Å, and c = 19.107 Å, with α = 96.062°, β = 92.66°, and γ = 90.011°. The structure is composed of double layers made of single oxygen, interconnected zig-zag chains made of square pyramids V(1)O<sub>5</sub>-V(2)O<sub>5</sub>-V(1)O<sub>5</sub> trimers, linked by tetrahedra-coordinated V(3)O<sub>4</sub>, placed between these upper and lower layers; the protonated H<sub>3</sub><sup>+</sup>NCH<sub>2</sub>CH<sub>2</sub>NH<sub>3</sub><sup>+</sup> diamines are intercalated between the layered stacked framework. The synthesis suggests a layered intercalation compound, H<sub>3</sub><sup>+</sup>NCH<sub>2</sub>CH<sub>2</sub>NH<sub>3</sub><sup>+</sup>-V<sub>2</sub>O<sub>5</sub>, is formed during the sol-gel process; the intermolecular forces previously discussed are key factors in obtaining both the layered intercalation compound and the squared microstructure; the reaction exhibits the ethylene diamine protonation with acetic acid.

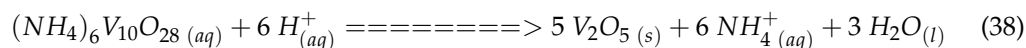
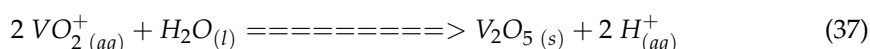
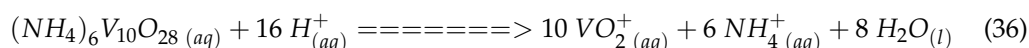
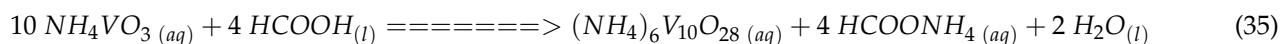


The final reduction and formation of (enH<sub>2</sub>)<sub>2</sub>V<sub>7</sub>O<sub>16</sub> is achieved by performing a hydrothermal treatment; the acetic acid concentration and protonated ethylenediamine will display the same NH<sub>4</sub><sup>+</sup> role previously observed in the (NH<sub>4</sub>)<sub>2</sub>V<sub>7</sub>O<sub>16</sub>; therefore, the acetic acid displays the reducing agent role to generate the mixed oxidation state, and the intercalated, protonated short-chain alkylamines will prevent the complete V<sub>2</sub>O<sub>5</sub> oxidant agent reduction. As the rolling effect is hindered, no tubular morphology is observed; the short length of the diamine is not enough to allow the nanotube formation; the 73.3% V<sup>4+</sup> and 26.7% V<sup>5+</sup> obtained gives the V<sup>4+</sup>/V<sup>5+</sup> ratio of 2.745, which is associated with a weighted oxidation state of 4.267+ (V<sup>4.267+</sup>). The reaction exhibits the redox process performed:

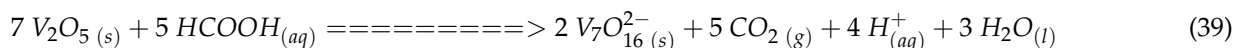


(En)<sub>2</sub>V<sub>7</sub>O<sub>16</sub> was previously reported by Worle et al. [72] unfortunately not in a pure phase. It was synthesized using the V<sup>5+</sup> VO(OCH(CH<sub>3</sub>)<sub>2</sub>)<sub>3</sub> precursor with ethylenediamine (H<sub>2</sub>NCH<sub>2</sub>CH<sub>2</sub>NH<sub>2</sub>), using a 2:1 molar ratio in ethanol and hydrolyzed with water. After aging for a day, a hydrothermal treatment was executed for seven days at 180 °C; the synthesis suggests the same V<sup>4+</sup> should be obtained in comparison with the aforementioned (EnH<sub>2</sub>)<sub>2</sub>V<sub>7</sub>O<sub>16</sub>. The structure has the same triclinic unit cell with red parameters: a = 6.16 Å, b = 6.17 Å, and c = 19.1 Å, with α = 96.14°, β = 92.82°, and γ = 90.07°, and presents the structural features previously mentioned.

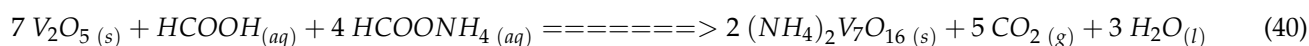
The micro-square morphology with the same lattice, (NH<sub>4</sub>)<sub>2</sub>V<sub>7</sub>O<sub>16</sub>, has been synthesized with different reducing agents. For example, Ma et al. [73,74] used the same V<sup>5+</sup> precursor (NH<sub>4</sub>VO<sub>3</sub>) without long or short alkyl chain primary monoamines/diamines but using formic acid HCOOH as the reducing agent in water instead. The mixture was hydrothermally aligned at 250 °C for 12 h; the reaction created micrometric square bricks. The first stage of the synthesis is very similar to the VO<sub>x</sub>-MSQ previously reviewed; the structural lattice was unknown and first described as novel—(NH<sub>4</sub>)<sub>2</sub>V<sub>2</sub>O<sub>5</sub>. In the synthesis, NH<sub>4</sub>VO<sub>3</sub> generates vanadates under various hydrolysis and condensation reactions; this is described in abbreviated form below, summarizing the possible processes that could be involved throughout the synthesis.



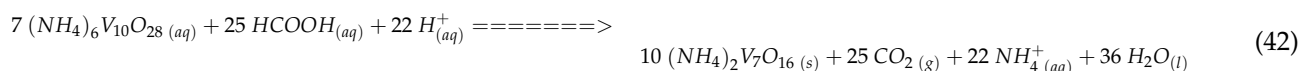
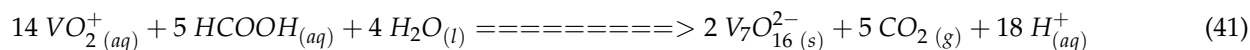
Decavanadate generates V<sub>2</sub>O<sub>5</sub> under precipitation at a low pH, which results in a reduction at a high temperature through the hydrothermal treatment, yielding the structural (NH<sub>4</sub>)<sub>2</sub>V<sub>7</sub>O<sub>16</sub> lattice with the micro-brick morphology; the redox reaction is listed below:



Considering the NH<sub>4</sub><sup>+</sup> polycations in aqueous media,



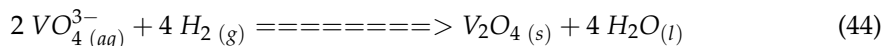
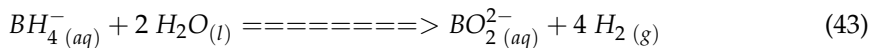
Some other reactions that could have taken place are listed below:



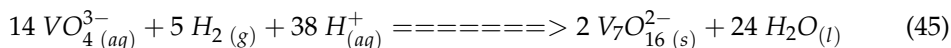
The V<sup>4+</sup>/V<sup>5+</sup> ratio is 0.667, approximately, yielding a 40.0% V<sup>4+</sup> content and a 60.0% V<sup>5+</sup> content. The weighted oxidation state is 4.60 (V<sup>4.60+</sup>), the smallest reduction degree in (NH<sub>4</sub>)<sub>2</sub>V<sub>7</sub>O<sub>16</sub> found in the literature. The structural lattice was resolved in their second work and resembles the same triclinic unit cell, framework, and red parameters previously described by Roppolo et al. [71] from the (EnH<sub>2</sub>)<sub>2</sub>V<sub>7</sub>O<sub>16</sub> microstructures.

Heo. et al. [75] reported the same micro-square (NH<sub>4</sub>)<sub>2</sub>V<sub>7</sub>O<sub>16</sub> morphology via a hydrothermal treatment at 250 °C for a period of time of 15 h, using the NH<sub>4</sub>VO<sub>3</sub> (V<sup>5+</sup> precursor) and LiBH<sub>4</sub> reducing agent in a tetrahydrofuran/water medium. Ammonium metavanadate in water exists in infinite tetrahedra chains; adjusting the pH will produce VO<sub>4</sub><sup>3-</sup> polyanion, which, in turn, is the main polyhedron in the equilibrium. Some previous

studies have demonstrated that LiAlBH<sub>4</sub> reduces VO<sub>4</sub><sup>3-</sup> polyoxoanions into VO<sub>2</sub>; therefore, a redox reaction could be associated with this transformation, considering the borohydride hydrolysis listed below:



The (NH<sub>4</sub>)<sub>2</sub>V<sub>7</sub>O<sub>16</sub> structural lattice could have been formed through many factors under the hydrothermal treatment; for example, with incomplete stoichiometry (adding minor quantities of LiAlBH<sub>4</sub>), VO<sub>4</sub><sup>3-</sup> will be partially reduced. Therefore, the formation of (NH<sub>4</sub>)<sub>2</sub>V<sub>7</sub>O<sub>16</sub> could be the main consequence, allowing the NH<sub>4</sub><sup>+</sup> intercalation inside the oxide layers; a reaction is exemplified below:

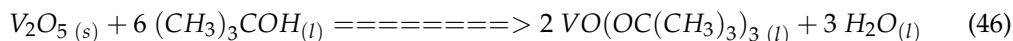


The V<sup>4+</sup>/V<sup>5+</sup> ratio is 2.45, approximately yielding a 71.0% V<sup>4+</sup> content and a 29.0% V<sup>5+</sup> content; the weighted oxidation state is 4.29 (V<sup>4.29+</sup>), similar to the BaV<sub>7</sub>O<sub>16</sub>•nH<sub>2</sub>O found in the literature. The structure features a triclinic unit cell with red parameters: a = 6.1480 Å, b = 6.1434 Å, and c = 18.0309 Å, with α = 95.621°, β = 93.018°, and γ = 89.971°. It displays the same framework and structural features previously mentioned by Wang et al. [65].

The previous method was optimized by Ma et al. [76] using the same V<sup>5+</sup> precursor (NH<sub>4</sub>VO<sub>3</sub>) dispersed in water, and reduced with LiBH<sub>4</sub> in tetrahydrofuran for 10 min. The black powder was transferred into a Teflon-lined autoclave and was hydrothermally treated for 10 h at 180 °C under low-speed rotation at 15 rpm; the (NH<sub>4</sub>)<sub>2</sub>V<sub>7</sub>O<sub>16</sub> microstructures display a hierarchical structure made of self-assembled nanoflakes resembling some sort of spheres. The V<sup>4+</sup>/V<sup>5+</sup> ratio is not informed, suggesting it has the same ratio informed in the previous method; the structural lattice framework and red parameters are equally related to (NH<sub>4</sub>)<sub>2</sub>V<sub>7</sub>O<sub>16</sub> ammonium vanadium bronze, reported by Heo et al. [75].

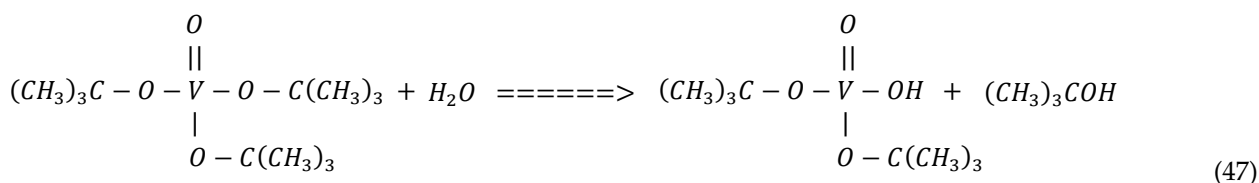
#### 4.4. Vanadium Oxide V<sub>6</sub>O<sub>11</sub> Rotationally Symmetric Nano Six-folds (VO<sub>x</sub>-NC) and Nano Star Fruits (VO<sub>x</sub>-NSF)

Vanadium oxide rotationally symmetric nano six-folds, featuring a star fruit or cog morphology (VO<sub>x</sub>-NC), were reported by O'Dwyer et al. [66]. The sol-gel synthesis employs vanadium oxide xerogel and long alkyl chain thiols; the layered vanadium oxide xerogel structure involves a reaction with a V<sub>2</sub>O<sub>5</sub> precursor, refluxed in tert-butanol for eight hours at 100 °C, approximately; the vanadium (V) tritertbutoxide is created, and the reaction is listed below:

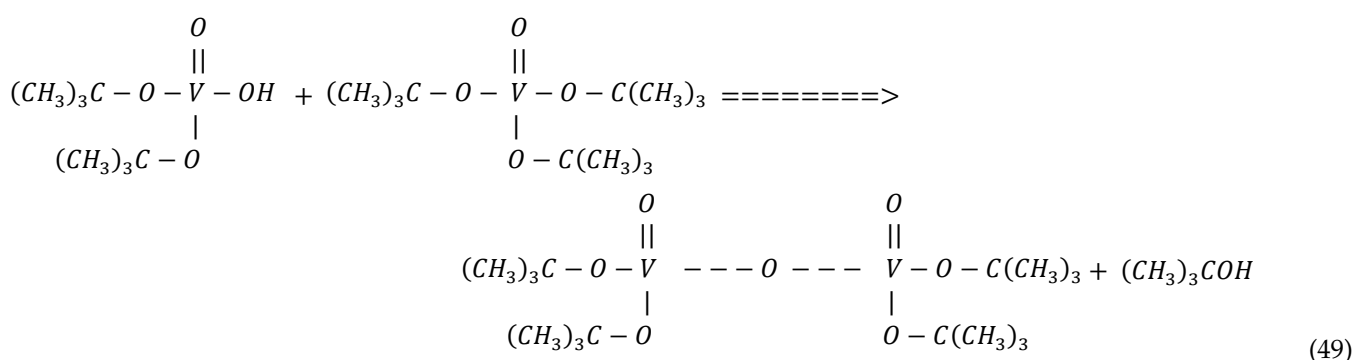
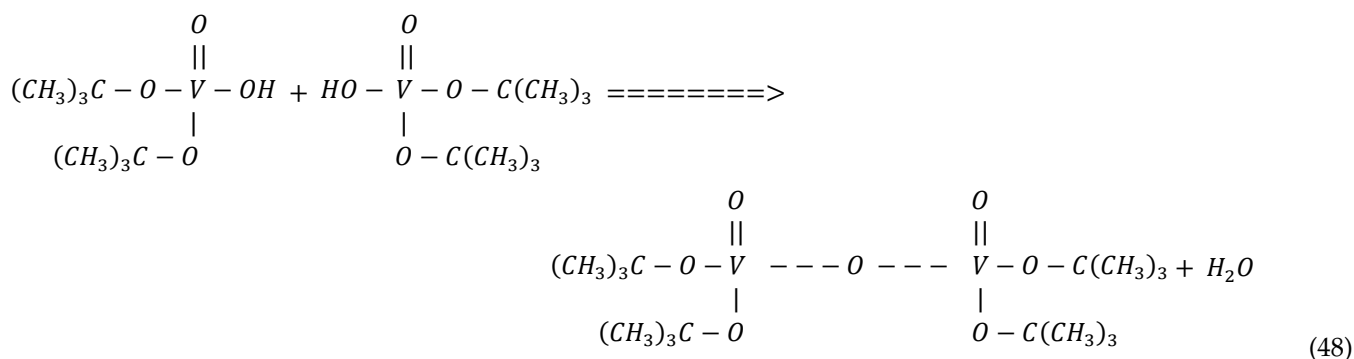


The VO(OC(CH<sub>3</sub>)<sub>3</sub>)<sub>3</sub> precursor reacts with water, generating the xerogel vanadium oxide (V<sub>2</sub>O<sub>5</sub>•nH<sub>2</sub>O)-layered compound, which becomes stable after rearrangement during an aging process of seven days. The xerogel structure is based on a sol-gel process, which is exhibited below:

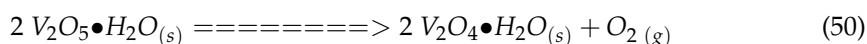
Hydrolysis



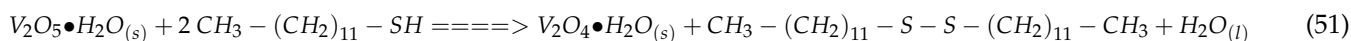
Condensation



It has been reported that xerogel encounters a small reduction process with water during the aging process; a simple reaction can exemplify this change:



There are some differences in the intercalation of the long alkyl chain thiols inside the vanadium oxide xerogel layers, when the reaction is performed at 40 °C instead. The organic functional group thiol, CH<sub>3</sub>-(CH<sub>2</sub>)<sub>11</sub>-SH (1-dodecanethiol (DDT)), is not able to interact with the host lattice under the hydrogen bonds, and the vanadium oxide content in xerogel is very low in comparison with other vanadium (V) oxide precursors; these factors might accelerate the reduction process during the early stage of the synthesis; therefore, the reaction could be represented below:



The temperature accelerates the reduction process, under vigorous stirring, and is associated with the self-assembled intercalated thiols. The interactions between the de vanadyl bonds from the host lattice are not strong enough, and are partially driven by the dipole–dipole interactions and London forces, which still allowed the intercalation compound formation, but failed to control the reduction path; therefore, the reduction degree is stronger; the reducing agent (thiols) might oxidate into disulphurs through the reaction; and the oxidant agent V<sub>2</sub>O<sub>5</sub> reduces halfway into V<sup>4+</sup>. The hydrothermal treatment over seven days at 180 °C increases the reduction process to an extensive degree; the structure changes from V<sub>2</sub>O<sub>5</sub>/V<sub>2</sub>O<sub>4</sub> into a crystalline V<sub>6</sub>O<sub>11</sub> lattice; the intermolecular forces are overcome; the thiol's oxidation into disulphurs allows the complete disintercalation process; the structure reduces the oxidation state into V<sup>3+</sup>/V<sup>4+</sup> mixture generating the star shape morphology. Two possible reactions can be seen below (considering the 180 °C temperature all-intercalated water had been removed from the xerogel). The SEM and TEM micrographs to appreciate the star morphology and the evidence of disintercalation signs

(also confirmed by XRD analysis) are displayed in Figures 8 and 9. More detailed scanning micrographs can be seen in the supporting information Figure S4.

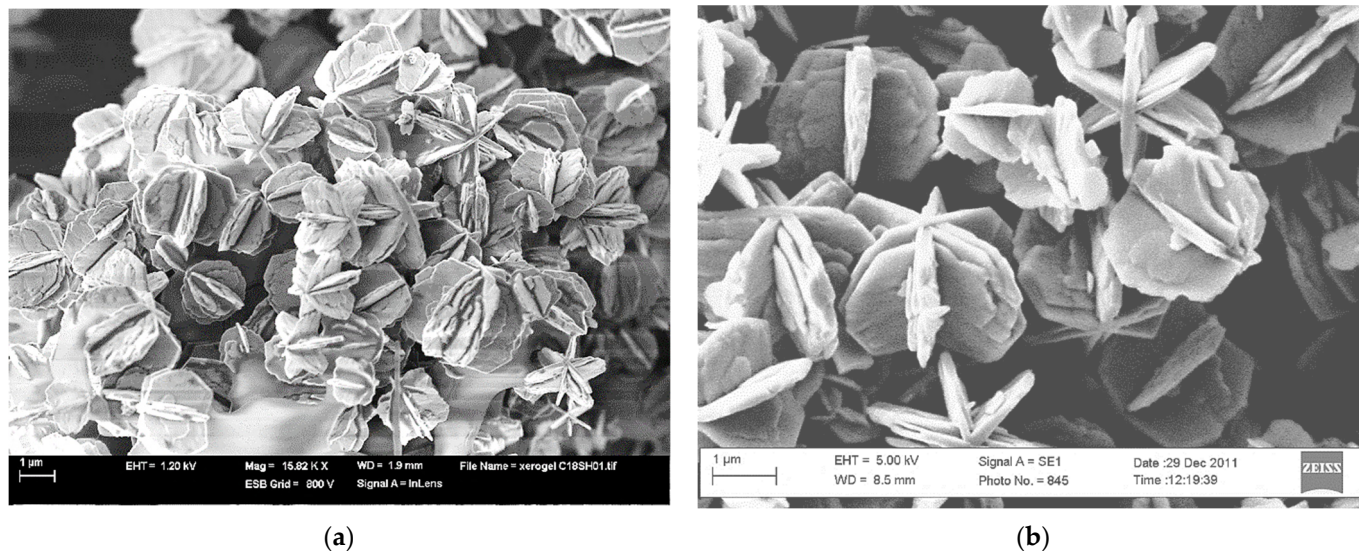
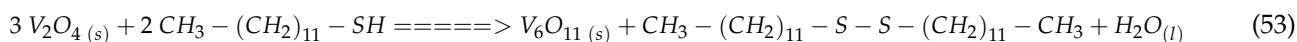
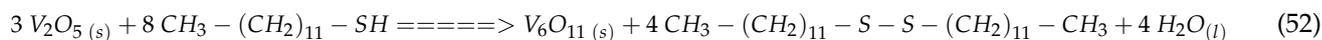


**Figure 8.** SEM micrographs of vanadium oxide  $\text{V}_6\text{O}_{11}$  rotationally symmetric six-folds (VOx-NC): (a) clustered  $\text{V}_6\text{O}_{11}$  vanadium oxide six-folds; (b) vanadium oxide six-folds, star-fruit morphology.

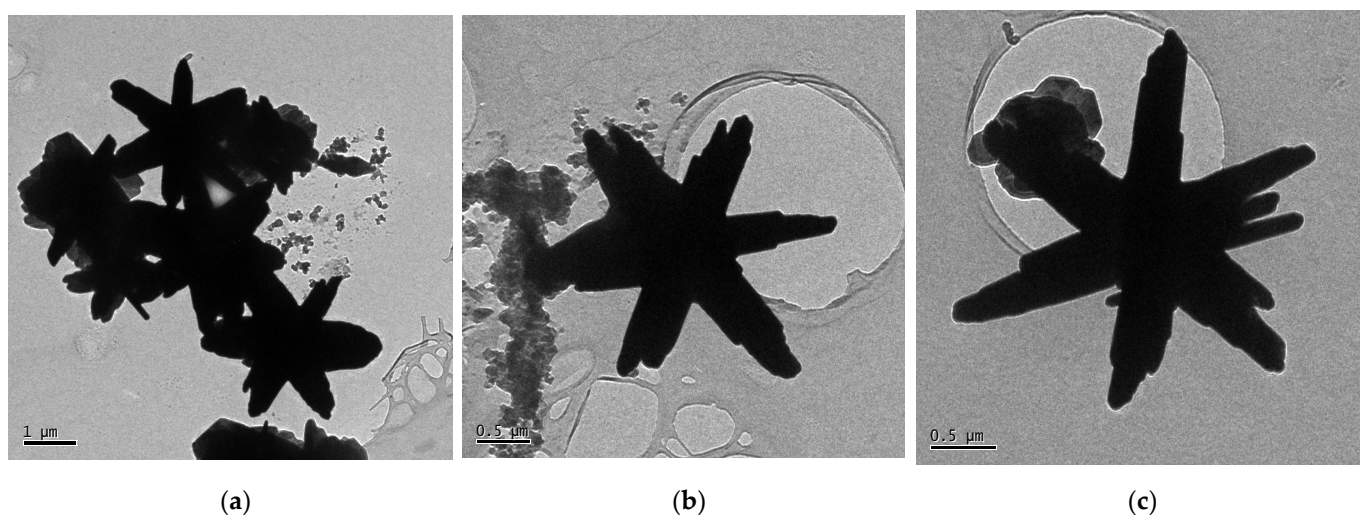


**Figure 9.** TEM micrographs of vanadium oxide  $\text{V}_6\text{O}_{11}$  rotationally symmetric six-folds (VOx-NC), the absence of pale fringes in the structures evidenced the disintercalation of long chain alkyl thiols: (a) clustered  $\text{V}_6\text{O}_{11}$  vanadium oxide six-folds; (b,c) isolated vanadium oxide six-folds.

The method to produce a similar structure with another structural lattice was reported by Shao et al. [67] The synthesis employed the vanadium oxide precursor  $\text{NH}_4\text{VO}_3$  in the presence of Pluronic 123; the pH was controlled with formic acid ( $\text{HCOOH}$ ); the mixture was hydrothermally aligned for 48 h at  $180^\circ\text{C}$ ; the hexangular star-fruit vanadium oxide obtained exhibits a  $\text{VO}_2$  structural lattice, confirming a full reduction from  $\text{V}^{5+}$  to  $\text{V}^{4+}$ . The first stage of the synthesis implies the transition from metavanadate into vanadium pentoxide at a lower pH under a sol-gel process; no evidence of an intercalation process is

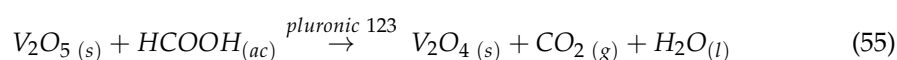
reported; therefore, at room temperature, the reduction process is minimal. The reaction below exhibits an abbreviated reaction.

First stage: Sol–gel



The second stage responds to the hydrothermal treatment, aided by two reducing agents, formic acid and Pluronic 123, and without the formation of an intercalation compound at the previous stage. Therefore, the oxidant agent reduction rate is faster at the same temperature used in the vanadium oxide VO<sub>x</sub>-MSQ previously described. The ammonium polycation (NH<sub>4</sub><sup>+</sup>) was not reported to be intercalated inside the vanadium dioxide in the final star-fruit structure, this suggests the ammonium stays as the HCOONH<sub>4</sub><sup>+</sup> salt during the hydrothermal treatment; the reaction can be seen below.

Hydrothermal treatment

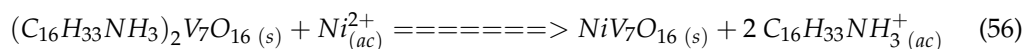


During the reduction, some nanosheets and nanofibers are made; therefore, the second role of the Pluronic 123 is to assist the self-assembly process of these nanostructures to build the final hexangular star-fruit structure.

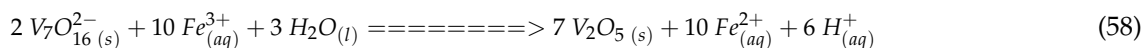
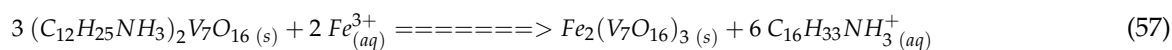
## 5. Mixed Oxidation States Rate Control

Researchers have tried to change or vary the V<sup>5+</sup>/V<sup>4+</sup> rate, in order to modify their electronic properties [77], without altering the structure morphology, and many applications and new properties have been enhanced and obtained. The most common techniques are functionalization processes on intercalated organic–inorganic hybrids, such as nanotubes or nanourchins. Some organic self-assembled amphiphilic molecules, foreign species such as cations, anions, and other surfactants, are reversibly inserted into the vanadium oxides sheets, regulating the oxidation state rate. Other techniques are doping processes such as adding or removing electrons, using reducing or oxidant agents, shifting the oxidation states rate; the synthesis can be modified in the beginning by adding small quantities of different metal cations to be part of the structure; the structure's morphology stays invariable but its electronic properties are adjusted; the atomic layer deposition (ALD) is used to achieve desirable electronic properties, as well; different atoms, cations, or anions are infiltrated in specific locations over the vanadium oxide microstructure without altering the structure's morphology. For example, V. Lavayen et al. [78] inserted gold nanoparticles (Au-NPs), stabilized with long alkyl thiols (1-dodecanethiol (DDT)), into vanadium oxide nanotubes (VO<sub>x</sub>-NTs) intercalated with 1-dodecylamine (DDA). The DDT: DDA of 4:1 (thiol:amine relationship) was refluxed with ethanol; Au-NPs were added in acetone under constant stirring; some amount of intercalated self-assembled DDA was replaced with self-assembled (Au-NPs)-DDT. TEM and electron diffraction were used to determine the two phases on the vanadium oxide nanowalls—one responding to the VO<sub>x</sub>-NTs/thiols and the other to the VO<sub>x</sub>-NT/Au-NPs inserted into the interlaminar spaces. The infrared FT spectroscopy features a vibration band at 962 cm<sup>−1</sup>, suggesting slightest quantities of V<sup>4+</sup> associated with a V<sup>4+</sup>/V<sup>5+</sup> rate modification; the replacement involves a decrease in intermolecular forces, mainly hydrogen bonds and ion-dipole interactions; the host lattice V<sub>7</sub>O<sub>16</sub><sup>2−</sup> experiences an oxidation process, shrinking the V<sup>4+</sup>/V<sup>5+</sup> ratio. Saleta et al. [79] studied the Ni<sup>2+</sup> influence on multiwall VO<sub>x</sub>-NTs; the self-assembled intercalated 1-hexadecylamine is exchanged with Ni<sup>2+</sup> cations in ethanol/water solvents without altering the tubular morphology; the magnetization characterizations exhibit a major decrease in V<sup>4+</sup> content from a ~50.0 to 16.0% (weighted oxidation state V<sup>4.5+</sup> to V<sup>4.88+</sup>); the effect was related to the disintercalated 1-hexadecylamine replaced by Ni<sup>2+</sup>

inside the  $V_7O_{16}^{2-}$  tubular layers, decreasing the interlayer distances and intermolecular forces. The next reaction exhibits the interexchange reaction:

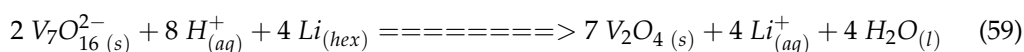


Zhang et al. [80] functionalized VOx-NTs  $(C_{12}H_{25}NH_3)_2V_7O_{16}$  made of  $V_2O_5$  precursor and 1-dodecylamine ( $C_{12}H_{25}NH_2$ ) with  $FeCl_3 \cdot 6H_2O$  aqueous solution under vigorous stirring, improving the electrochemical performance. The intercalated self-assembled  $C_{12}H_{25}NH_3^+$  are interexchanged with the  $Fe^{3+}$  cation; the process decreased the interlayer distances in the VOx-NTs multiwall and the  $V^{4+}$  content due to the disintercalation/intercalation of the self-assembled  $C_{12}H_{25}NH_3^+/Fe^{3+}$  cations. The  $V^{4+}/V^{5+}$  ratio shifts from 1.07 regular VOx-NTs (51.79%  $V^{4+}$  and 48.21%  $V^{5+}$ ) content and weighted oxidation state of  $V^{4.482+}$  to a 0.883 ratio ( $Fe^{3+}, Fe^{2+}C_{12}H_{25}NH_3^+$ )( $V_7O_{16}$ )<sub>3</sub> VOx-NTs (46.9%  $V^{4+}$  and 53.1%  $V^{5+}$ ) content featuring an average oxidation state of  $V^{4.531+}$ . A set of reactions exhibits these processes, assuming the first step is a simple interexchange reaction, and the second step is associated to a redox process:

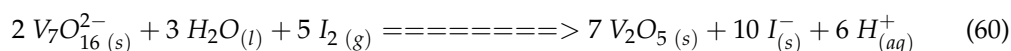


Saliman et al. [81] obtained Zr-doped VOx-NTs, employing the  $V_2O_5$  precursor with 1-dodecylamine ( $C_{12}H_{25}NH_2$ ) and adding a slight amount of  $ZrO_2$ ; all the reagents were mixed in water until a gel was formed. The  $(C_{12}H_{25}NH_3)_2V_{6,86}Zr_{0,02}O_{16}$  nanotubes containing 2.0%  $Zr^{4+}$  dopant were obtained under hydrothermal treatment over four days at 180 °C. The interlayer distances shifted from 2.65 nm to 2.70 nm; the increase corresponds to the  $V^{5+}$  replacement with  $Zr^{4+}$ , which features a larger ionic radius (0.80 Å) than  $V^{5+}$  (0.50 Å); therefore, the  $V^{5+}$  content decreased, and the  $V^{4+}/V^{5+}$  ratio should have increased, as well; the tubular morphology has remained without collapsing the structure.

The charged electron and hole-doping functionalization has also been successfully performed by Krusin-Elbaum et al. [82]. The electron functionalization was performed on  $(C_{12}H_{25}NH_3)_2V_7O_{16}$  nanotubes; the butyl lithium solution employed contains the necessary amount of lithium to compensate each  $V^{5+}$  cation to reduce it into  $V^{4+}$ ; the  $V^{4+}/V^{5+}$  ratio increases considerably and ferromagnetic behavior is observed at room temperature. A simple reaction can exemplify the process, assuming some intercalated water belongs from the VOx-NTs.

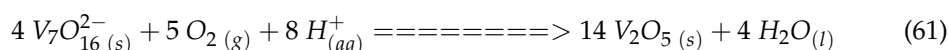


This method was performed under the same fashion, but the lithium ions are intercalated through an interexchange reaction with the self-assembled long alkyl chains primary monoamines, the intercalated lithium ions stabilize the  $V^{4+}/V^{5+}$  ratio, decreasing the  $V^{4+}$  content, and high temperature ferromagnetism arises from the Li-VO<sub>x</sub> NTs with specific amounts of intercalated lithium ions [83]. The other charge doping functionalization performed by Krusin-Elbaum was hole-doping, employing certain amounts of sublimated iodine for different periods of time to extract electrons from the  $V^{4+}$  (V (3) centers); the production of holes eradicates the spin frustration from the VOx-NTs system; the  $V^{4+}/V^{5+}$  ratio decreases and room temperature ferromagnetism arises, as well. A simple reaction can explain the redox process, assuming there is some intercalated water inside the VOx-NTs.



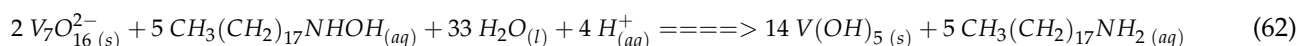
Saleta et al. [84] conducted research on VOx-NTs aging time; it was found that the vanadyl bond  $V^{4+} = O$  oxidizes to  $V^{5+} = O$ , changing drastically the  $V^{4+}/V^{5+}$  ratio; therefore, the magnetic properties suffer forceful changes; the variation throughout the aging time

suggests that oxidation might be the key factor in all the different  $V^{4+}$  content values reported in the literature. These were obtained employing different quantification methods; the aging process studied over 65 months at environmental conditions (room temperature and pressure) exhibits the oxidation from 70.0% to 12.0%  $V^{4+}$  content using the XANES technique; the oxidation changes the  $V^{4+}/V^{5+}$  ratio from 2.33 to 0.136; therefore, the weighted oxidation state in each case is  $V^{4.30+}$  in brand-new  $V^{4.88+}$  in aged VOx-NTs; even though the increased oxidation of 58.0% is radical, the tubular morphology remains intact; the reaction can be seen below.



## 6. Morphologic Defects

Structural morphologic defects might be involved in some redox processes of vanadium oxide microstructures. The reduction could increase or decrease, depending on the type of defect. For example, defect-rich VOx-NTs [69] have smaller amounts of  $V^{4+}$  content than regular VOx-NTs, and the different magnetic properties are related to these defects. The effect is accomplished when the amount of surfactant (reducing agent) is decreased; the mol stoichiometry used to achieve the effect is 2:1. ( $V_2O_5$ - $C_{18}H_{37}NH_2$  (1-octadecylamine)); defect-rich  $(C_{18}H_{37}NH_3)_2V_7O_{16}$  VOx-NTs exhibits a 1/3  $V^{4+}/V^{5+}$  ratio, resulting in a  $V^{4.75+}$  weighted oxidation state, featuring 25.0%  $V^{4+}$  and 75.0%  $V^{5+}$  content, respectively, in comparison to conventional  $(C_{18}H_{37}NH_3)_2V_7O_{16}$  VOx-NTs with a 1/2  $V^{4+}/V^{5+}$  ratio, which corresponds to 33.45%  $V^{4+}$  and 66.55%  $V^{5+}$  content. The weighted oxidation state in defect-rich VOx-NTs is  $V^{4.666+}$ , and the defects are oxygen vacancies; the formation of O- $V^{5+}$ -OH hydroxyl groups with 60.0% content causes the V (3) tetrahedral  $V^{4+}$  site to face oxidation in the  $V_7O_{16}^{2-}$  structural lattice. The vanadyl bond,  $V^{4+} = O$ , transitions to  $V^{5+}$ -OH in the defect-rich VOx-NTs in comparison with the 30.0% hydroxyl groups exhibited in the 1/2 ratio  $V^{4+}/V^{5+}$  VOx-NTs regular sample. The reaction below explains the possible oxidation:



The next set of micrographs in Figure 10 exhibits some structural morphologic defects in  $(NH_4)_2V_7O_{16}$  MSQ, with the eroded borders displaying a high degree of porosity, and  $(C_{18}H_{35}NH_3)_2V_7O_{16}$  NU displaying a surface crack that was obtained through the hydrothermal treatment, which might also change the  $V^{4+}/V^{5+}$  ratio. Other SEM and TEM micrographs from defect VOx-microstructures are featured in the supporting information in Figures S5 and S6.

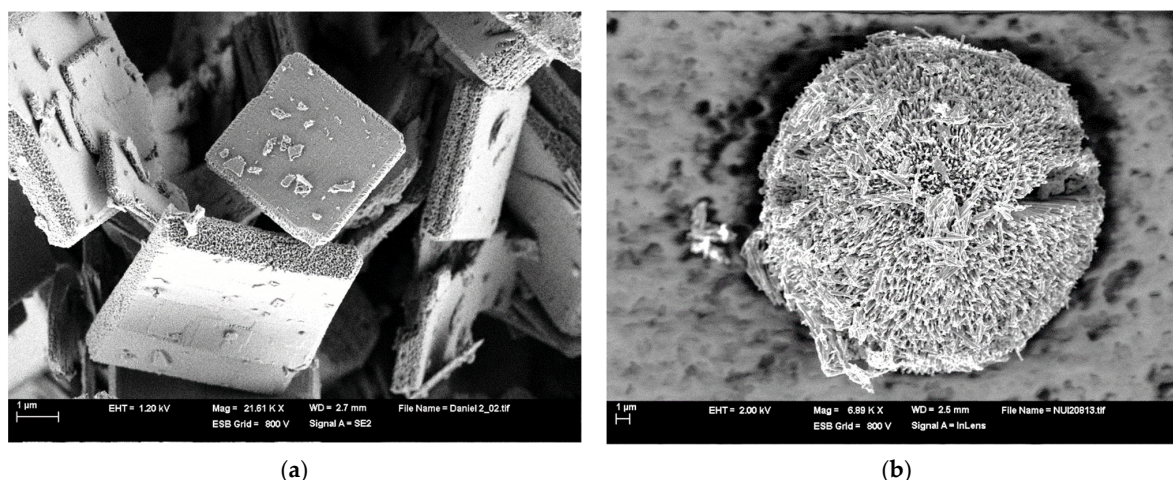


**Figure 10.** SEM micrographs of defected vanadium oxide  $(NH_4)_2V_7O_{16}$  micro-squares (VOx-MSQ): (a) general view of clustered and eroded VOx-MSQ featuring borders with high porosity degree; (b) cracked  $(C_{18}H_{35}NH_3)_2V_7O_{16}$  nanourchins (VOx-NU).

## 7. Conclusions

Vanadium oxide microstructures with mixed oxidation states are frequently obtained under sol–gel processes enhanced with hydrothermal treatment. Intercalation processes using functional groups such as long alkyl chain primary monoamines or ammonium cations regulate the vanadium oxidation states in different proportions. For urchins and nanotubes containing self-assembled long alkyl chain primary amines, the  $V^{4+}/V^{5+}$  ratio is around 0.85 (46.0%  $V^{4+}$  and 54.0%  $V^{5+}$ ); for a layered square morphology intercalated with ammonium cations, the  $V^{4+}/V^{5+}$  rate is around 2.70 (73.0%  $V^{4+}$  and 27.0%  $V^{5+}$ ); in other vanadium oxide microstructures where no intercalation compounds are obtained during hydrothermal treatment, such as symmetric rotationally six-folds and hexangular star-fruits, the reductions go even further; in the case of six-folds, a mixed oxidation states rate  $V^{3+}/V^{4+}$  is generated, and, for star-fruits and micrometric crosses, a solely oxidation state  $V^{4+}$  is developed.

Intermolecular forces are fundamental to the intercalation processes and perhaps control the oxidation states rate, such as dipole–dipole and ion–dipole; nevertheless, stronger intermolecular forces such as hydrogen bonds display a major role for urchins, squares, and nanotubes, where multiple interactions occur inside the vanadium oxide layers during the sol–gel process. The  $V^{5+}$  oxidation state remains constant throughout the hydrothermal treatment; the London forces between the self-assembled long alkyl chains. The ion–dipole and cooperative hydrogen bond interactions between the primary monoamines functional groups with the vanadyl bonds of the host  $V_7O_{16}^{2-}$  structural lattice are enough to maintain the  $V^{4+}/V^{5+}$  ratio at 1.0 in the nanotubes and urchins. In the square morphology, cooperative hydrogen bonds between the ammonium cation with the vanadyl bonds from the  $V_7O_{16}^{2-}$  host lattice increases the  $V^{4+}/V^{5+}$  ratio to 2.70. An analogous effect arises with intercalated protonated ethylene diamines, in addition displaying the same behavior with the vanadyl bonds from the  $V_7O_{16}^{2-}$  host lattice, if the synthesis pH is performed at pH lower than 6. The three vanadium oxide microstructures will produce mixed oxidation states.

If the intercalation processes do not prevail during the hydrothermal treatment, or were not developed during the first stage of the synthesis, the reduction processes are straightforward, depending on factors such as: the functional group of the surfactant, vanadium oxide ( $V_2O_5$ ) precursor concentration, temperature, and reaction time used previously in the sol–gel processes, and, during the hydrothermal treatment, a complete reduction from  $V^{5+}$  to  $V^{4+}$  emerge in structures such as hexangular star-fruits, vanadium oxide crosses ( $VO_2$  or  $V_2O_4$ ). The reduction degree is even higher in rotationally symmetric six-folds ( $V_6O_{11}$ ), which exhibit a  $V^{3+}/V^{4+}$  ratio.

Vanadium oxide chemistry exhibits multivariant equilibria involving most of the ionic equilibria such as acid–base, coordination, solubility, and redox, associated with different structural lattices.

**Supplementary Materials:** The following supporting information can be downloaded at: <https://www.mdpi.com/article/10.3390/reactions4010001/s1>, Figure S1. SEM Micrographs VOx-NU; Figure S2. SEM Micrographs VOx-MC; Figure S3. TEM micrographs VOx-MC; Figure S4. SEM Micrographs VOx-MC; Figure S5. SEM Micrographs of defect VOx-MSQ and VOx-NU; Figure S6. TEM Micrographs of defect VOx-MSQ.

**Author Contributions:** Conceptualization, methodology, resources, writing—original draft preparation, writing—review and editing, visualization, supervision, funding acquisition, D.N. All authors have read and agreed to the published version of the manuscript.

**Funding:** This research received no external funding.

**Data Availability Statement:** Not applicable.

**Conflicts of Interest:** The authors declare no conflict of interest.

## References

1. Mounasamy, V.; Mani, G.K.; Madanagurusamy, S. Vanadium oxide nanostructures for chemiresistive gas and vapour sensing: A review on state of the art. *Microchim. Acta* **2020**, *187*, 1–29. [[CrossRef](#)]
2. Yang, F.; Zhu, Y.; Xia, Y.; Xiang, S.; Han, S.; Cai, C.; Wang, Q.; Wang, Y.; Gu, M. Fast Zn<sup>2+</sup> kinetics of vanadium oxide nanotubes in high-performance rechargeable zinc-ion batteries. *J. Power Sources* **2020**, *451*, 227767. [[CrossRef](#)]
3. Mousavi, S.M. Vanadium oxide nanotubes for selective catalytic reduction of NO<sub>x</sub> with NH<sub>3</sub>. *Chin. J. Chem. Eng.* **2016**, *24*, 914–919. [[CrossRef](#)]
4. Zhou, X.; He, T.; Chen, X.; Zhao, Z.; Guo, X.; Sun, L.; Liu, Z. Synthesis and lithium storage properties of vanadium oxide nanotubes (VO<sub>x</sub>-NTs)-Polyaniline nanocomposite as cathode material for lithium ion batteries. *J. Mater. Sci. Mater. Electron.* **2017**, *28*, 11098–11107. [[CrossRef](#)]
5. Pinheiro, A.L.G.; do Carmo, J.V.C.; Carvalho, D.C.; Oliveira, A.C.; Rodríguez-Castellón, E.; Tehuacanero-Cuapa, S.; Otubo, L.; Lang, R. Bio-additive fuels from glycerol acetalization over metals-containing vanadium oxide nanotubes (MeVO<sub>x</sub>-NT in which, Me = Ni, Co, or Pt). *Fuel Processing Technol.* **2019**, *184*, 45–56. [[CrossRef](#)]
6. Fang, D.; Li, L.; Xu, W.; Li, G.; Luo, Z.; Liang, C.; Ji, Y.; Xu, J.; Xiong, C. Self-assembled hairy ball-like V<sub>2</sub>O<sub>5</sub> nanostructures for lithium ion batteries. *RSC Adv.* **2014**, *4*, 25205–25209. [[CrossRef](#)]
7. Yu, W.; Wang, J.; Gou, Z.; Zeng, W.; Guo, W.; Lin, L. Hydrothermal synthesis of vanadium pentoxide nanostructures and their morphology control. *Ceram. Int.* **2013**, *39*, 2639–2643. [[CrossRef](#)]
8. Shoorangiz, M.; Shariatifard, L.; Roshan, H.; Mirzaei, A. Hydrothermally synthesized flower-like vanadium oxide nanostructures for ethanol sensing studies. *Mater. Sci. Semicond. Processing* **2022**, *137*, 106241. [[CrossRef](#)]
9. Nefzi, H.; Sediri, F. Vanadium oxide nanourchins: Hydrothermal synthesis, characterization, frequency dependent electrical properties. *Ceram. Int.* **2015**, *41*, 1391–1399. [[CrossRef](#)]
10. Chandrappa, G.T.; Steunou, N.; Cassaignon, S.; Bauvais, C.; Biswas, P.K.; Livage, J. Vanadium Oxide: From Gels to Nanotubes. *J. Sol-Gel Sci. Technol.* **2003**, *26*, 593–596. [[CrossRef](#)]
11. Liu, M.; Su, B.; Tang, Y.; Jiang, X.; Yu, A. Recent Advances in Nanostructured Vanadium Oxides and Composites for Energy Conversion. *Adv. Energy Mater.* **2017**, *7*, 1700885. [[CrossRef](#)]
12. Sahraeian, N.; Esmailzadeh, F.; Mowla, D. Hydrothermal synthesis of V<sub>2</sub>O<sub>5</sub> nanospheres as catalyst for hydrogen sulfide removal from sour water. *Ceram. Int.* **2021**, *47*, 923–934. [[CrossRef](#)]
13. Faggio, G.; Modafferi, V.; Panzera, G.; Alfieri, D.; Santangelo, S. Micro-Raman and photoluminescence analysis of composite vanadium oxide/poly-vinyl acetate fibres synthesised by electro-spinning. *J. Raman Spectrosc.* **2012**, *43*, 761–768. [[CrossRef](#)]
14. Bieri, F.; Krumeich, F.; Muhr, H.-J.; Nesper, R. The First Vanadium Oxide Nanotubes Containing an Aromatic Amine as Template. *Helv. Chim. Acta* **2001**, *84*, 3015–3022. [[CrossRef](#)]
15. Niederberger, M.; Muhr, H.-J.; Krumeich, F.; Bieri, F.; Günther, D.; Nesper, R. Low-Cost Synthesis of Vanadium Oxide Nanotubes via Two Novel Non-Alkoxide Routes. *Chem. Mater.* **2000**, *12*, 1995–2000. [[CrossRef](#)]
16. Chen, X.; Sun, X.; Li, Y. Self-Assembling Vanadium Oxide Nanotubes by Organic Molecular Templates. *Inorg. Chem.* **2002**, *41*, 4524–4530. [[CrossRef](#)]
17. Zhang, Y. Synthesis and phase transition properties of VO<sub>2</sub> (M) hollow spheres with large thermal hysteresis width. *Micro Nano Lett.* **2019**, *14*, 819–822. [[CrossRef](#)]
18. Xu, Y.; Deng, X.; Li, Q.; Zhang, G.; Xiong, F.; Tan, S.; Wei, Q.; Lu, J.; Li, J.; An, Q.; et al. Vanadium Oxide Pillared by Interlayer Mg<sup>2+</sup> Ions and Water as Ultralong-Life Cathodes for Magnesium-Ion Batteries. *Chem* **2019**, *5*, 1194–1209. [[CrossRef](#)]
19. Inagaki, M.; Nakamura, T.; Shimizu, A. Soft process for the intercalation of ammonium cations into vanadium oxide. *J. Mater. Res.* **1998**, *13*, 896–900. [[CrossRef](#)]
20. Rojas-Cervantes, M.L.; Casal, B.; Aranda, P.; Savirón, M.; Galván, J.C.; Ruiz-Hitzky, E. Hybrid materials based on vanadium pentoxide intercalation complexes. *Colloid Polym. Sci.* **2001**, *279*, 990–1004. [[CrossRef](#)]
21. Clites, M.; Pomerantseva, E. Bilayered vanadium oxides by chemical pre-intercalation of alkali and alkali-earth ions as battery electrodes. *Energy Storage Mater.* **2018**, *11*, 30–37. [[CrossRef](#)]
22. López-Cabaña, Z.; Navas, D.; Benavente, E.; Ana, M.A.S.; Lavayen, V.; González, G. Hybrid Lamellar Organic-Inorganic Semiconducting Nanocomposites. *Mol. Cryst. Liq. Cryst.* **2012**, *554*, 119–134. [[CrossRef](#)]
23. Gannon, G.; O'Dwyer, C.; Larsson, J.A.; Thompson, D. Interdigitating Organic Bilayers Direct the Short Interlayer Spacing in Hybrid Organic-Inorganic Layered Vanadium Oxide Nanostructures. *J. Phys. Chem. B* **2011**, *115*, 14518–14525. [[CrossRef](#)] [[PubMed](#)]
24. Krumeich, F.; Muhr, H.J.; Niederberger, M.; Bieri, F.; Reinoso, M.; Nesper, R. Vanadium Oxide Nanotubes with Diamine Templates. *MRS Online Proc. Libr.* **1999**, *581*, 393–398. [[CrossRef](#)]
25. Durupthy, O.; Steunou, N.; Coradin, T.; Livage, J. Intercalation of dipeptides during V<sub>2</sub>O<sub>5</sub>•nH<sub>2</sub>O xerogel condensation. *J. Phys. Chem. Solids* **2006**, *67*, 944–949. [[CrossRef](#)]
26. Zhang, Y.; Du, Y.; Song, B.; Wang, Z.; Wang, X.; Wan, F.; Ma, X. Manganese-ions and polyaniline co-intercalation into vanadium oxide for stable zinc-ion batteries. *J. Power Sources* **2022**, *545*, 231920. [[CrossRef](#)]

27. Roy, A.; Pradhan, M.; Ray, C.; Sahoo, R.; Dutta, S.; Pal, T. Facile synthesis of pyridine intercalated ultra-long V<sub>2</sub>O<sub>5</sub> nanowire from commercial V<sub>2</sub>O<sub>5</sub>: Catalytic applications in selective dye degradation. *CrystEngComm* **2014**, *16*, 7738–7744. [[CrossRef](#)]
28. Zabrodina, G.S.; Makarov, S.G.; Kremlev, K.V.; Yunin, P.A.; Gusev, S.A.; Kaverin, B.S.; Kaverina, L.B.; Ketkov, S.Y. Novel hybrid materials based on the vanadium oxide nanobelts. *Appl. Surf. Sci.* **2016**, *368*, 395–402. [[CrossRef](#)]
29. Zhou, X.; Chen, X.; He, T.; Bi, Q.; Sun, L.; Liu, Z. Fabrication of polypyrrole/vanadium oxide nanotube composite with enhanced electrochemical performance as cathode in rechargeable batteries. *Appl. Surf. Sci.* **2017**, *405*, 146–151. [[CrossRef](#)]
30. Mai, L.; Chen, W.; Xu, Q.; Zhu, Q.; Han, C.; Peng, J. Cost-saving synthesis of vanadium oxide nanotubes. *Solid State Commun.* **2003**, *126*, 541–543. [[CrossRef](#)]
31. Nadimicherla, R.; Liu, Y.; Chen, K.; Chen, W. Effect of polyethylene glycol on vanadium oxide nanotubes in lithium-ion batteries. *Microelectron. Eng.* **2014**, *127*, 81–85. [[CrossRef](#)]
32. Kweon, H.; Lee, K.W.; Lee, C.E. Ferromagnetism in water-doped vanadium oxide nanotubes. *J. Appl. Phys.* **2010**, *108*, 023905. [[CrossRef](#)]
33. Emmerich, J.; Dillen, M.; Kirschhock, C.E.A.; Martens, J.A. Fine-tuning of Vanadium Oxide Nanotubes. In *Studies in Surface Science and Catalysis*; Gaigneaux, E.M., Devillers, M., Hermans, S., Jacobs, P.A., Martens, J.A., Ruiz, P., Eds.; Elsevier: Amsterdam, The Netherlands, 2010; Volume 175, pp. 249–252.
34. Nordlinder, S.; Augustsson, A.; Schmitt, T.; Guo, J.; Duda, L.C.; Nordgren, J.; Gustafsson, T.; Edström, K. Redox Behavior of Vanadium Oxide Nanotubes As Studied by X-ray Photoelectron Spectroscopy and Soft X-ray Absorption Spectroscopy. *Chem. Mater.* **2003**, *15*, 3227–3232. [[CrossRef](#)]
35. Nefzi, H.; Sediri, F. Vanadium oxide nanotubes VO<sub>x</sub>-NTs: Hydrothermal synthesis, characterization, electrical study and dielectric properties. *J. Solid State Chem.* **2013**, *201*, 237–243. [[CrossRef](#)]
36. Li, Z.; Zhang, Y.; Shi, Z. Hydrothermal synthesis of nanowires, nanobelts, and nanotubes of vanadium oxides from one reaction system. *Int. J. Mater. Res.* **2013**, *104*, 567–572. [[CrossRef](#)]
37. Huang, Z.; Zeng, H.; Xue, L.; Zhou, X.; Zhao, Y.; Lai, Q. Synthesis of vanadium oxide, V<sub>6</sub>O<sub>13</sub> hollow-flowers materials and their application in electrochemical supercapacitors. *J. Alloy. Compd.* **2011**, *509*, 10080–10085. [[CrossRef](#)]
38. Wu, C.; Wei, H.; Ning, B.; Xie, Y. New Vanadium Oxide Nanostructures: Controlled Synthesis and Their Smart Electrical Switching Properties. *Adv. Mater.* **2010**, *22*, 1972–1976. [[CrossRef](#)]
39. Zavalij, P.Y.; Whittingham, M.S. Structural chemistry of vanadium oxides with open frameworks. *Acta Crystallogr. Sect. B* **1999**, *55*, 627–663. [[CrossRef](#)]
40. Przeźniak-Welenc, M.; Łapiński, M.; Lewandowski, T.; Kościelska, B.; Wicikowski, L.; Sadowski, W. The Influence of Thermal Conditions on V<sub>2</sub>O<sub>5</sub> Nanostructures Prepared by Sol-Gel Method. *J. Nanomater.* **2015**, *2015*. [[CrossRef](#)]
41. Petkov, V.; Trikalitis, P.N.; Bozin, E.S.; Billinge, S.J.L.; Vogt, T.; Kanatzidis, M.G. Structure of V<sub>2</sub>O<sub>5</sub>•nH<sub>2</sub>O Xerogel Solved by the Atomic Pair Distribution Function Technique. *J. Am. Chem. Soc.* **2002**, *124*, 10157–10162. [[CrossRef](#)]
42. Timmerman, M.A.; Xia, R.; Le, P.T.P.; Wang, Y.; ten Elshof, J.E. Metal Oxide Nanosheets as 2D Building Blocks for the Design of Novel Materials. *Chem.—A Eur. J.* **2020**, *26*, 9084–9098. [[CrossRef](#)] [[PubMed](#)]
43. Saini, M.; Dehiya, B.S.; Umar, A.; Goyat, M.S. Phase modulation in nanocrystalline vanadium di-oxide (VO<sub>2</sub>) nanostructures using citric acid via one pot hydrothermal method. *Ceram. Int.* **2019**, *45*, 18452–18461. [[CrossRef](#)]
44. Soltane, L.; Sediri, F. Hydrothermal synthesis and characterization of mesoporous rod-like hybrid organic-inorganic nanocrystalline based vanadium oxide. *Ceram. Int.* **2014**, *40*, 1531–1538. [[CrossRef](#)]
45. Liang, X.; Gao, G.; Wu, G.; Yang, H. Synthesis and characterization of novel hierarchical starfish-like vanadium oxide and their electrochemical performance. *Electrochim. Acta* **2016**, *188*, 625–635. [[CrossRef](#)]
46. Mjeiri, I.; Etteyeb, N.; Sediri, F. Mesoporous vanadium oxide nanostructures: Hydrothermal synthesis, optical and electrochemical properties. *Ceram. Int.* **2014**, *40*, 1387–1397. [[CrossRef](#)]
47. Li, G.; Chao, K.; Peng, H.; Chen, K.; Zhang, Z. Low-Valent Vanadium Oxide Nanostructures with Controlled Crystal Structures and Morphologies. *Inorg. Chem.* **2007**, *46*, 5787–5790. [[CrossRef](#)]
48. Livage, J. Hydrothermal Synthesis of Nanostructured Vanadium Oxides. *Materials* **2010**, *3*, 4175–4195. [[CrossRef](#)]
49. Subba Reddy, C.V.; Mho, S.-i.; Kalluru, R.R.; Williams, Q.L. Hydrothermal synthesis of hydrated vanadium oxide nanobelts using poly (ethylene oxide) as a template. *J. Power Sources* **2008**, *179*, 854–857. [[CrossRef](#)]
50. Grigorieva, A.V.; Goodilin, E.A.; Anikina, A.V.; Kolesnik, I.V.; Tretyakov, Y.D. Surfactants in the formation of vanadium oxide nanotubes. *Mendeleev. Commun.* **2008**, *18*, 71–72. [[CrossRef](#)]
51. Chandrappa, G.T.; Steunou, N.; Cassaignon, S.; Bauvais, C.; Livage, J. Hydrothermal synthesis of vanadium oxide nanotubes from V<sub>2</sub>O<sub>5</sub> gels. *Catal. Today* **2003**, *78*, 85–89. [[CrossRef](#)]
52. Li, H.-Y.; Qiu, X.; Dong, M.; Li, X.; Zhang, Y.; Xie, B. Tuned hydrothermal synthesis of vanadium dioxide nanotubes. *Ceram. Int.* **2015**, *41*, 13967–13973. [[CrossRef](#)]
53. Vo, T.N.; Kim, H.; Hur, J.; Choi, W.; Kim, I.T. Surfactant-assisted ammonium vanadium oxide as a superior cathode for calcium-ion batteries. *J. Mater. Chem. A* **2018**, *6*, 22645–22654. [[CrossRef](#)]
54. Wang, X.; Liu, L.; Jacobson, A.J. Electrochemical-hydrothermal synthesis and structure determination of a novel layered mixed-valence oxide: BaV<sub>7</sub>O<sub>16</sub>•nH<sub>2</sub>O. *Chem. Commun.* **1998**, *9*, 1009–1010. [[CrossRef](#)]

55. Petkov, V.; Zavalij, P.Y.; Lutta, S.; Whittingham, M.S.; Parvanov, V.; Shastri, S. Structure beyond Bragg: Study of V<sub>2</sub>O<sub>5</sub> nanotubes. *Phys. Rev. B* **2004**, *69*, 085410. [[CrossRef](#)]
56. Hellmann, I.; Täschner, C.; Klingeler, R.; Leonhardt, A.; Büchner, B.; Knupfer, M. Structure and electronic properties of Li-doped vanadium oxide nanotubes. *J. Chem. Phys.* **2008**, *128*, 224701. [[CrossRef](#)] [[PubMed](#)]
57. McNulty, D.; Buckley, D.N.; O'Dwyer, C. Synthesis and electrochemical properties of vanadium oxide materials and structures as Li-ion battery positive electrodes. *J. Power Sources* **2014**, *267*, 831–873. [[CrossRef](#)]
58. Krumeich, F.; Muhr, H.J.; Niederberger, M.; Bieri, F.; Schnyder, B.; Nesper, R. Morphology and Topochemical Reactions of Novel Vanadium Oxide Nanotubes. *J. Am. Chem. Soc.* **1999**, *121*, 8324–8331. [[CrossRef](#)]
59. Nordlinder, S.; Lindgren, J.; Gustafsson, T.; Edström, K. The Structure and Electrochemical Performance of Na<sup>+</sup>, K<sup>+</sup>, and Ca<sup>2+</sup> Vanadium Oxide Nanotubes. *J. Electrochem. Soc.* **2003**, *150*, E280. [[CrossRef](#)]
60. Liu, A.; Ichihara, M.; Honma, I.; Zhou, H. Vanadium-oxide nanotubes: Synthesis and template-related electrochemical properties. *Electrochem. Commun.* **2007**, *9*, 1766–1771. [[CrossRef](#)]
61. Huang, C.; Liu, X.; Kong, L.; Zhou, H.; Liu, Y.; Qiu, J.; Wang, Y. Hydrothermal synthesis of vanadium oxide nanotubes by a facile route. *Rare Met.* **2006**, *25*, 88–93. [[CrossRef](#)]
62. Navas, D.; Fuentes, S.; Castro-Alvarez, A.; Chavez-Angel, E. Review on Sol-Gel Synthesis of Perovskite and Oxide Nanomaterials. *Gels* **2021**, *7*, 275. [[CrossRef](#)] [[PubMed](#)]
63. Perera, S.D.; Patel, B.; Bonso, J.; Grunewald, M.; Ferraris, J.P.; Balkus, K.J., Jr. Vanadium Oxide Nanotube Spherical Clusters Prepared on Carbon Fabrics for Energy Storage Applications. *ACS Appl. Mater. Interfaces* **2011**, *3*, 4512–4517. [[CrossRef](#)] [[PubMed](#)]
64. Navas, D.; Donoso, J.P.; Magon, C.; Sotomayor-Torres, C.M.; Moreno, M.; Lozano, H.; Benavente, E.; González, G. Ammonium hexadeca-oxo-heptavanadate microsquares. A new member in the family of the V<sub>7</sub>O<sub>16</sub> mixed-valence nanostructures. *New J. Chem.* **2019**, *43*, 17548–17556. [[CrossRef](#)]
65. Wang, Z.; Zhang, J.; Wang, H.; Wei, X.; Zhang, J.; Chen, H.; Liu, S.; Wei, S.; Lu, X. Hydrothermal synthesis of ammonium vanadate [(NH<sub>4</sub>)<sub>2</sub>V<sub>7</sub>O<sub>16</sub>•3.6 H<sub>2</sub>O] as a promising zinc-ion cathode: Experimental and theoretical study of its storage. *Electrochim. Acta* **2022**, *404*, 139785. [[CrossRef](#)]
66. O'Dwyer, C.; Lavayen, V.; Fuenzalida, D.; Newcomb, S.B.; Santa Ana, M.A.; Benavente, E.; González, G.; Sotomayor Torres, C.M. Six-fold rotationally symmetric vanadium oxide nanostructures by a morphotropic phase transition. *Phys. Status Solidi (b)* **2007**, *244*, 4157–4160. [[CrossRef](#)]
67. Shao, J.; Li, X.; Qu, Q.; Zheng, H. One-step hydrothermal synthesis of hexangular starfruit-like vanadium oxide for high power aqueous supercapacitors. *J. Power Sources* **2012**, *219*, 253–257. [[CrossRef](#)]
68. Saleta, M.E.; Aurelio, G.; Bardelli, F.; Sánchez, R.D.; Malta, M.; Torresi, R.M. The local environment of Co<sup>2+</sup> ions intercalated in vanadium oxide/hexadecylamine nanotubes. *J. Phys. Condens. Matter* **2012**, *24*, 435302. [[CrossRef](#)]
69. Won Lee, K.; Kweon, H.; Lee, C.E. Electron spin resonance of defect-rich vanadium oxide nanotubes. *J. Appl. Phys.* **2009**, *106*, 044313. [[CrossRef](#)]
70. O'Dwyer, C.; Navas, D.; Lavayen, V.; Benavente, E.; Santa Ana, M.A.; González, G.; Newcomb, S.B.; Sotomayor Torres, C.M. Nano-Urchin: The Formation and Structure of High-Density Spherical Clusters of Vanadium Oxide Nanotubes. *Chem. Mater.* **2006**, *18*, 3016–3022. [[CrossRef](#)]
71. Roppolo, M.; Jacobs, C.B.; Upreti, S.; Chernova, N.A.; Whittingham, M.S. Synthesis and characterization of layered and scrolled amine-templated vanadium oxides. *J. Mater. Sci.* **2008**, *43*, 4742–4748. [[CrossRef](#)]
72. Wörle, M.; Krumeich, F.; Bieri, F.; Muhr, H.-J.; Nesper, R. Flexible V<sub>7</sub>O<sub>16</sub> Layers as the Common Structural Element of Vanadium Oxide Nanotubes and a New Crystalline Vanadate. *Z. Für Anorg. Allg. Chem.* **2002**, *628*, 2778–2784. [[CrossRef](#)]
73. Ma, Y.; Ji, S.; Zhou, H.; Zhang, S.; Li, R.; Zhu, J.; Li, W.; Guo, H.; Jin, P. Synthesis of novel ammonium vanadium bronze (NH<sub>4</sub>)<sub>0.6</sub>V<sub>2</sub>O<sub>5</sub> and its application in Li-ion battery. *RSC Adv.* **2015**, *5*, 90888–90894. [[CrossRef](#)]
74. Ma, Y.; Wu, M.; Jin, X.; Shu, R.; Hu, C.; Xu, T.; Li, J.; Meng, X.; Cao, X. (NH<sub>4</sub>)<sub>2</sub>V<sub>7</sub>O<sub>16</sub> Microbricks as a Novel Anode for Aqueous Lithium-Ion Battery with Good Cyclability. *Chem.—A Eur. J.* **2021**, *27*, 12341–12351. [[CrossRef](#)] [[PubMed](#)]
75. Heo, J.W.; Bu, H.; Hyoung, J.; Hong, S.-T. Ammonium Vanadium Bronze, (NH<sub>4</sub>)<sub>2</sub>V<sub>7</sub>O<sub>16</sub>, as a New Lithium Intercalation Host Material. *Inorg. Chem.* **2020**, *59*, 4320–4327. [[CrossRef](#)] [[PubMed](#)]
76. Ma, Y.; Shu, R.; Xu, T.; Li, J.; Zhu, D.; Jin, X.; Wu, M.; Cao, X. Self-assembled (NH<sub>4</sub>)<sub>2</sub>V<sub>7</sub>O<sub>16</sub> hierarchical structures with improved electrochemical performance for aqueous Li-ion batteries. *New J. Chem.* **2021**, *45*, 20099–20102. [[CrossRef](#)]
77. Jacobs, C.; Roppolo, M.; Butterworth, K.; Ban, C.; Chernova, N.A.; Whittingham, M.S. Magnetic Properties of Vanadium Oxide Nanotubes, Nanourchins, and Nanorods. *MRS Online Proc. Libr.* **2007**, *988*. [[CrossRef](#)]
78. Lavayen, V.; O'Dwyer, C.; Cárdenas, G.; González, G.; Sotomayor Torres, C.M. Towards thiol functionalization of vanadium pentoxide nanotubes using gold nanoparticles. *Mater. Res. Bull.* **2007**, *42*, 674–685. [[CrossRef](#)]
79. Saleta, M.E.; Curiale, J.; Troiani, H.E.; Ribeiro Guevara, S.; Sánchez, R.D.; Malta, M.; Torresi, R.M. Influence of Ni doping on vanadium oxide/hexadecylamine multiwall nanotubes. *Phys. B Condens. Matter.* **2007**, *398*, 333–336. [[CrossRef](#)]
80. Zhang, K.; Gao, G.; Sun, W.; Liang, X.; Liu, Y.; Wu, G. Large interlayer spacing vanadium oxide nanotubes as cathodes for high performance sodium ion batteries. *RSC Adv.* **2018**, *8*, 22053–22061. [[CrossRef](#)]
81. Azita Saliman, H.R.A.; Ketabi, S. Synthesis and Characterization of Zr-Doped Vanadium Oxide Nanotubes. *Am. J. Chem. Eng.* **2018**, *6*, 49–53. [[CrossRef](#)]

82. Krusin-Elbaum, L.; News, D.M.; Zeng, H.; Derycke, V.; Sun, J.Z.; Sandstrom, R. Room-temperature ferromagnetic nanotubes controlled by electron or hole doping. *Nature* **2004**, *431*, 672–676. [[CrossRef](#)] [[PubMed](#)]
83. Popa, A.I.; Vavilova, E.; Arango, Y.C.; Kataev, V.; Täschner, C.; Klauss, H.H.; Maeter, H.; Luetkens, H.; Büchner, B.; Klingeler, R. High-temperature ferromagnetism of Li-doped vanadium oxide nanotubes. *EPL* **2009**, *88*, 57002. [[CrossRef](#)]
84. Saleta, M.E.; Tobia, D.; Figueroa, S.J.A.; López, C.A.; Granada, M.; Sánchez, R.D.; Malta, M.; Torresi, R.M. Aging effect on vanadium oxide hybrid nanotubes. *J. Phys. Condens. Matter* **2019**, *31*, 505701. [[CrossRef](#)] [[PubMed](#)]

**Disclaimer/Publisher’s Note:** The statements, opinions and data contained in all publications are solely those of the individual author(s) and contributor(s) and not of MDPI and/or the editor(s). MDPI and/or the editor(s) disclaim responsibility for any injury to people or property resulting from any ideas, methods, instructions or products referred to in the content.